Coarse Graining Empirical Densities and Currents in Continuous-Space Steady States

Cai Dieball and Aljaž Godec*
Mathematical bioPhysics Group, Max Planck Institute for Multidisciplinary Sciences, Am Faßberg 11, 37077 Göttingen

We present the conceptual and technical background required to describe and understand the correlations and fluctuations of the empirical density and current of steady-state diffusion processes on all time scales — observables central to statistical mechanics and thermodynamics on the level of individual trajectories. We focus on the important and non-trivial effect of a spatial coarse graining. Making use of a generalized time-reversal symmetry we provide deeper insight about the physical meaning of fluctuations of the coarse-grained empirical density and current, and explain why a systematic variation of the coarse-graining scale offers an efficient method to infer bounds on a system's dissipation. Moreover, we discuss emerging symmetries in the statistics of the empirical density and current, and the statistics in the large deviations regime. More broadly our work promotes the application of stochastic calculus as a powerful direct alternative to Feynman-Kac theory and path-integral methods.

I. INTRODUCTION

A non-vanishing probability current [1–17] and entropy production [18–27] are the hallmarks of non-equilibrium, manifested as transients during relaxation [25–31] or in non-equilibrium, current-carrying steady states [4–6, 32–34]. Genuinely irreversible, detailed balance violating dynamics emerge in the presence of non-conservative forces (e.g. shear or rotational flow) [35–38] or active driving in living matter fueled by ATP-hydrolysis [16, 39–46]. Such systems are typically small and "soft", and thus subject to large thermal fluctuations. Single-molecule [45–49] and particle-tracking [50] experiments probe dynamical processes on the level of individual, stochastic trajectories. These are typically analyzed within the framework of "time-average statistical mechanics" [5, 50–56], i.e. by averaging along individual finite realizations yielding random quantities with nontrivial statistics.

Ergodic steady states are characterized by the (invariant) steady-state density $p_{\rm s}(\mathbf{x})$ and a steady-state probability current $\mathbf{j}_{\rm s}(\mathbf{x})$ in systems with a broken detailed balance. One can equivalently infer $p_{\rm s}(\mathbf{x})$ and $\mathbf{j}_{\rm s}(\mathbf{x})$ from an ensemble of statistically independent trajectories of an ergodic process, or from an individual but very long (i.e. ergodically long [57]) trajectory. To infer $p_{\rm s}(\mathbf{x})$ and $\mathbf{j}_{\rm s}(\mathbf{x})$ from individual sample paths one uses estimators that are called the *empirical density* and *empirical current*, respectively, defined as

$$\begin{aligned}\overline{\rho_{\mathbf{x}}^{U}}(t) &\equiv \frac{1}{t}\int_0^t U_{\mathbf{x}}^h(\mathbf{x}_\tau)d\tau \\ \overline{\mathbf{J}_{\mathbf{x}}^{U}}(t) &\equiv \frac{1}{t}\int_{\tau=0}^{\tau=t} U_{\mathbf{x}}^h(\mathbf{x}_\tau)\circ d\mathbf{x}_\tau,\end{aligned} \tag{1}$$

where $U_{\mathbf{x}}^h(\mathbf{z})$ is a "window function" around a point $\mathbf{x}$ with a characteristic scale h [58] and $\circ\, d\mathbf{x}_\tau$ denotes the Stratonovich integral, which both will be specified more precisely below. Notably, the Stratonovich integration $\circ d\mathbf{x}_\tau$ in Eq. (1) is the correct way to make sense of the expression "$\dot{\mathbf{x}}_\tau d\tau$", which is ill-defined since for any τ with probability one $|\dot{\mathbf{x}}_\tau| = \infty$ for overdamped Langevin dynamics [59]. Because $(\mathbf{x}_\tau)_{0\le\tau\le t}$ is random, $\overline{\rho_{\mathbf{x}}^{U}}(t)$ and $\overline{\mathbf{J}_{\mathbf{x}}^{U}}(t)$ are fluctuating quantities. Notably, the empirical density and current are typically defined with a delta function, i.e. with $U_{\mathbf{x}}^{h\to 0}(\mathbf{z}) = \delta(\mathbf{x}-\mathbf{z})$. For a variety of reasons detailed in the accompanying letter [58] we here define $U_{\mathbf{x}}^h$ with a finite length scale $h > 0$, such that $\overline{\rho_{\mathbf{x}}^{U}}(t)$ measures the time spent in the region $U_{\mathbf{x}}^h$ around $\mathbf{x}$ and $\overline{\mathbf{J}_{\mathbf{x}}^{U}}(t)$ the displacements in the region $U_{\mathbf{x}}^h$ around $\mathbf{x}$. Such a definition is in line with that of generalized currents in stochastic thermodynamics [5, 52–54] except that we here consider vector-valued currents. Important recent results on such generalized currents (however, without the notion of coarse graining) may be found in [15, 55, 56, 60, 61].

The fluctuations of $\overline{\rho_{\mathbf{x}}^{U}}(t)$ and $\overline{\mathbf{J}_{\mathbf{x}}^{U}}(t)$ may be interpreted as variances of fluctuating histograms. Namely, after "binning" into (hyper)volumes around points $\mathbf{x}$ (or in our language the coarse-graining around $\mathbf{x}$), often carried out on a grid, each individual trajectory yields a random histogram of occupation fractions or displacements. That is, the height of bins in the histogram reflects the time spent or displacement in said bin accumulated over all visits of the trajectory until time t for $\overline{\rho_{\mathbf{x}}^{U}}(t)$ and $\overline{\mathbf{J}_{\mathbf{x}}^{U}}(t)$, respectively, and is a fluctuating quantity due to the stochasticity of trajectories. The variance of these fluctuations quantifies the inference uncertainty. In Fig. 1 we show such histograms inferred from individual trajectories of a two-dimensional harmonically confined overdamped diffusion in a rotational flow

$$d\mathbf{x}_t = -\begin{bmatrix}1 & -\Omega\\ \Omega & 1\end{bmatrix}\mathbf{x}dt + \sqrt{2}d\mathbf{W}_t, \tag{2}$$

with Gaussian window

$$U_{\mathbf{x}}^h(\mathbf{z}) = \frac{1}{2\pi h^2}\exp\left[-\frac{(\mathbf{z}-\mathbf{x})^2}{2h^2}\right]. \tag{3}$$

* agodec@mpinat.mpg.de

For this process and window function we analytically solved all spatial integrals [58] entering the results derived below, and numerically evaluated one remaining time-integral.

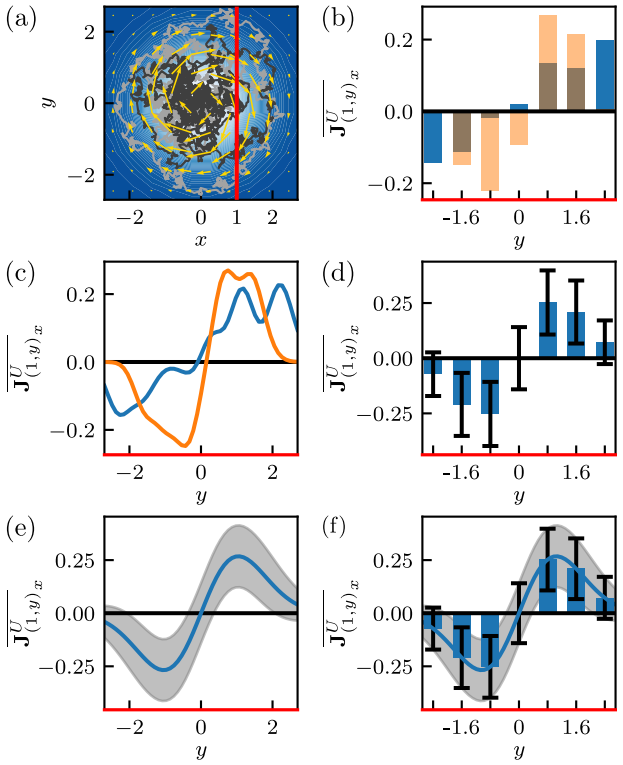

FIG. 1. (a) Two trajectories (gray) with length $t = 5$ in harmonically confined rotational flow Eq. (2) with $\Omega = 5$. The steady-state density and current are depicted by the color gradient and yellow arrows, respectively. (b) Height of bins depict the time-averaged x-component of the current with Gaussian coarse-graining window Eq. (3) with $h = 0.3$ evaluated for several points on the red line in (a) for the two trajectories in (a). This corresponds to time-averaging all local displacements (weighted by $U^h_{\mathbf{x}}$) within a single trajectory. (c) As in (b) but for the continuum of points on the red line in (a). This can be considered as the x-component of the current smoothened over a scale h. (d) Mean value $\langle A\rangle_{\mathrm{s}}$ and standard deviation $\sqrt{\mathrm{var(A)}}$ of $A = \overline{\mathbf{J}^U_{(1,y)}}_x$ obtained from our result Eq. (50). This represents the statistics of many histograms as in (b). (e) As in (d) but for continuous y as in (c). (f) Overlaying (d) and (e) shows that the histogram picture is fully contained in the continuous coarse graining procedure.

The interpretation of the coarse graining captured in or induced by $U^h_{\mathbf{x}}$ in Eq. (1) is flexible; it can represent a projection or a "generalized current" [5, 15, 52–56, 60, 61] or may be thought of as a spatial smoothing of the empirical current and density as shown in Fig. 1c,e and Fig. 2, also for the case of a finite experimental resolution. Our main focus here is the smoothing aspect in the context of uncertainty of $p_{\mathrm{s}}(\mathbf{x}), \mathbf{j}_{\mathrm{s}}(\mathbf{x})$ and steady-state dissipation from individual trajectories. Note that some form of coarse graining or smoothing is in fact required in order for the quantities in Eq. (1) to be well defined [58]. A suitable smoothing decreases the uncertainty of the estimate and, if varied over sufficiently many h and $\mathbf{x}$ (see also Fig. 1c,e) instead of simply "binning", one does not necessarily lose information (as compared to input data). Moreover, a systematic variation of the scale h may reveal more information about $\overline{\rho^U_{\mathbf{x}}}(t)$ and $\overline{\mathbf{J}^U_{\mathbf{x}}}(t)$. The same reasoning is found to apply to generalized thermodynamic currents and allows for an improved inference of dissipation, see [58] and below.

The present work is an extended exposé of the conceptual and technical background that is required to understand and materialize the above observations. It accompanies the letter [58] but does not duplicate any information. Several additional explanations, illustrations and applications are given here.

The article is structured as follows. In Sec. II we lay out the theoretical background on stochastic differential equations in the Itô, Stratonovich and anti-Itô interpretations and the corresponding equations for the probability densities. We furthermore decompose the drift and steady-state current into conservative and non-conservative (i.e. irreversible) contributions and introduce dissipation. In Sec. III we prove a generalize time-reversal symmetry called "dual-reversal symmetry". In Sec. IV we derive our main results for the steady-state (co)variances of $\overline{\rho^U_{\mathbf{x}}}(t)$ and $\overline{\mathbf{J}^U_{\mathbf{x}}}(t)$ and interpret them in terms of initial- and end-point currents and increments. In Sec. V we use current fluctuations to infer steady-state dissipation via the Thermodynamic Uncertainty Relation (TUR) [15, 34] with an emphasis on the importance of the coarse-graining scale h. In particular we demonstrate and explain the existence of a thermodynamically optimal coarse graining. In Sec. VI we discuss symmetries obeyed by the (co)variances and explain how the results simplify in thermodynamic equilibrium. In Sec. VII we present asymptotic results for short and long trajectories and give results for large deviation theory. We conclude with a summary and perspectives for the future.

II. THEORY

A. Set-up – overdamped Langevin dynamics

In this chapter we provide background on the equations of motion for the coordinate $\mathbf{x}_\tau$ highlighting the differences between the Itô, Stratonovich, and anti-Itô interpretations, and for their corresponding conditional probability density functions of a transition $\mathbf{x}_0 \to \mathbf{x}$.

We consider time-homogeneous (i.e. coefficients do not explicitly depend on time) overdamped Langevin dynamics in d-dimensional space with (possibly) multiplicative noise [62, 63] described by the thermodynamically consistent [20, 64] anti-Itô (or Hänggi-Kilmontovich [65, 66]) stochastic differential equation

$$d\mathbf{x}_\tau = \mathbf{F}(\mathbf{x}_\tau)d\tau + \boldsymbol{\sigma}(\mathbf{x}_\tau) \circledast d\mathbf{W}_\tau, \tag{4}$$

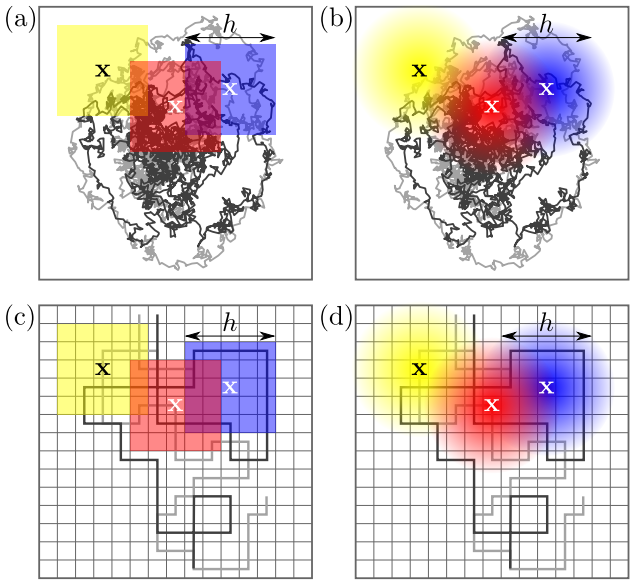

FIG. 2. (a) Coarse-graining windows (colors) in the form of an indicator function of a rectangle centered at different points $\mathbf{x}$ with coarse-graining scale h. For each $\mathbf{x}$ and h, each trajectory (gray lines) gives rise to one value for the (coarse grained) time-averaged density and current. Note that the choice of $\mathbf{x}$ and h is flexible such that the windows may overlap. (b) Same as (a) but with Gaussian coarse-graining windows. (c-d) Coarse-graining windows in the case of trajectory data with a finite experimental resolution (grid, gray trajectories). The coarse graining scale h should be chosen large compared to the resolution to obtain reliable approximations of the (coarse-grained) densities and currents.

where $d\mathbf{W}_\tau$ is the increment of a d-dimensional Wiener processes (i.e. white noise) with zero mean and covariance $\langle dW_{\tau,i} dW_{\tau',j}\rangle = \delta(\tau-\tau')\delta_{ij}d\tau$. The noise amplitude is related to the diffusion coefficient via $\mathbf{D}(\mathbf{x}) \equiv \boldsymbol{\sigma}(\mathbf{x})\boldsymbol{\sigma}(\mathbf{x})^T/2$. We assume the drift field $\mathbf{F}(\mathbf{x})$ to be smooth and sufficiently confining, such that the anti-Itô (end-point) convention $\circledast d\mathbf{W}_\tau = \mathbf{W}_\tau - \mathbf{W}_{\tau-d\tau}$ guarantees the existence of a steady-state probability density $p_\mathrm{s}(\mathbf{x}) = \mathrm{e}^{-\phi(\mathbf{x})}$ and steady-state current $\mathbf{j}_\mathrm{s}(\mathbf{x})$, and yields Boltzmann-Gibbs (equilibrium) statistics when $\mathbf{D}(\mathbf{x})^{-1}\mathbf{F}(\mathbf{x}) = -\nabla\phi(\mathbf{x})$ is a potential force.

The anti-Itô equation (4) can equivalently be rewritten as an Itô equation with an adapted drift as,

$$\begin{aligned} d\mathbf{x}_t &= \mathbf{F}(\mathbf{x}_t)dt + \boldsymbol{\sigma}(\mathbf{x}_t) \circledast d\mathbf{W}_t \\ &= \mathbf{F}(\mathbf{x}_t)dt + \left[\left\{\nabla^T\sqrt{2\mathbf{D}(\mathbf{x}_t)}\right\}d\mathbf{x}_t\right]\cdot d\mathbf{W}_t \\ &\quad + \sqrt{2\mathbf{D}(\mathbf{x}_t)}d\mathbf{W}_t \\ &= \left[\mathbf{F}(\mathbf{x}_t) + \left\{\nabla^T\mathbf{D}\right\}(\mathbf{x}_t)\right]dt + \sqrt{2\mathbf{D}(\mathbf{x}_t)}d\mathbf{W}_t, \end{aligned} \tag{5}$$

where the brackets $\{\cdot\}$ throughout denote that the differential operator only acts within the bracket and $\sqrt{2\mathbf{D}(\mathbf{x}_t)}$ represents the matrix $\boldsymbol{\sigma}(\mathbf{x}_t)$. At this point several remarks are in order. First, the anti-Itô interpretation of the stochastic differential equation (4) as well as the Stratonovich integral in Eq. (1) are both required for thermodynamic consistency. Second, there is no difference between the interpretations of Eq. (4) if $\mathbf{D}(\mathbf{x}) = \mathbf{D}$ is a constant matrix, i.e. the convention only matters for multiplicative noise. However, even in this case the Stratonovich integral in Eq. (1) is required for thermodynamic consistency of the empirical current and to use it as an estimator of $\mathbf{j}_\mathrm{s}(\mathbf{x})$.

Since the process is ergodic the drift allows for a unique decomposition into reversible $\mathbf{F}^\mathrm{rev}(\mathbf{x}) = -\mathbf{D}(\mathbf{x})\{\nabla\phi\}(\mathbf{x})$ and irreversible $\mathbf{F}^\mathrm{irrev}(\mathbf{x}) = p_\mathrm{s}^{-1}(\mathbf{x})\mathbf{j}_\mathrm{s}(\mathbf{x})$ parts that are orthogonal, i.e. $\mathbf{F}^\mathrm{rev}(\mathbf{x})\cdot\mathbf{F}^\mathrm{irrev}(\mathbf{x}) = 0$ [26, 67]. This implies that the steady-state density $p_\mathrm{s}(\mathbf{x})$ is not altered by $\mathbf{F}^\mathrm{irrev}(\mathbf{x})$ and the steady-state current lies tangentially to hypersurfaces with constant $p_\mathrm{s}(\mathbf{x})$, i.e. tangentially to equipotential lines in the two-dimensional case.

The Fokker-Planck equation for the conditional probability density $G(\mathbf{x},t|\mathbf{y})$ to be at a point $\mathbf{x}$ at time t after starting at $\mathbf{y}$ that corresponds to Eqs. (4) and (5) reads

$$\begin{aligned} \partial_t G(\mathbf{x},t|\mathbf{y}) &= [-\nabla_\mathbf{x}\cdot\mathbf{F}(\mathbf{x}) + \nabla_\mathbf{x}^T\mathbf{D}(\mathbf{x})\nabla_\mathbf{x}]G(\mathbf{x},t|\mathbf{y}) \\ &\equiv L(\mathbf{x})G(\mathbf{x},t|\mathbf{y}), \end{aligned} \tag{6}$$

which satisfies a continuity equation $(\partial_t + \nabla_\mathbf{x}\cdot\hat{\mathbf{j}}_\mathbf{x})G(\mathbf{x},t|\mathbf{y}) = 0$, where

$$\hat{\mathbf{j}}_\mathbf{x} \equiv \mathbf{F}(\mathbf{x}) - \mathbf{D}(\mathbf{x})\nabla_\mathbf{x}. \tag{7}$$

The decomposition of the drift translates to a decomposition of $\hat{\mathbf{j}}_\mathbf{x}$ into a gradient part $\hat{\mathbf{j}}^g(\mathbf{x})$ and steady-state-current contributions, namely $\hat{\mathbf{j}}_\mathbf{x} = \mathbf{F}^\mathrm{irrev}(\mathbf{x}) + \mathbf{F}^\mathrm{rev}(\mathbf{x}) - \mathbf{D}(\mathbf{x})\nabla_\mathbf{x}$ is rewritten using

$$\begin{aligned} \hat{\mathbf{j}}^g(\mathbf{x}) &\equiv \mathbf{F}^\mathrm{rev}(\mathbf{x}) - \mathbf{D}(\mathbf{x})\nabla \\ &= \mathbf{D}(\mathbf{x})\left\{\nabla\log(p_\mathrm{s}(\mathbf{x})\right\} - \mathbf{D}(\mathbf{x})\nabla \\ &= \mathbf{D}(\mathbf{x})p_\mathrm{s}^{-1}(\mathbf{x})\left\{\nabla p_\mathrm{s}(\mathbf{x})\right\} - \mathbf{D}(\mathbf{x})\nabla \\ &= -\mathbf{D}(\mathbf{x})\left[p_\mathrm{s}(\mathbf{x})\{\nabla p_\mathrm{s}^{-1}(\mathbf{x})\} - \nabla\right] \\ &= -\mathbf{D}(\mathbf{x})p_\mathrm{s}(\mathbf{x})\nabla p_\mathrm{s}^{-1}(\mathbf{x}), \end{aligned} \tag{8}$$

where we have used that $\{\nabla p_\mathrm{s}(\mathbf{x})^{-1}\} = -p_\mathrm{s}^{-2}(\mathbf{x})\{\nabla p_\mathrm{s}\}(\mathbf{x})$ implies $\{\nabla p_\mathrm{s}\}(\mathbf{x}) = -p_\mathrm{s}^2(\mathbf{x})\{\nabla p_\mathrm{s}^{-1}\}(\mathbf{x}))$. Thus we obtain

$$\begin{aligned} \hat{\mathbf{j}}_\mathbf{x} &= \hat{\mathbf{j}}^g_\mathbf{x} + p_\mathrm{s}^{-1}(\mathbf{x})\mathbf{j}_\mathrm{s}(\mathbf{x}) \\ &= -p_\mathrm{s}(\mathbf{x})\mathbf{D}(\mathbf{x})\nabla_\mathbf{x}p_\mathrm{s}^{-1}(\mathbf{x}) + p_\mathrm{s}^{-1}(\mathbf{x})\mathbf{j}_\mathrm{s}(\mathbf{x}), \end{aligned} \tag{9}$$

where $\mathbf{j}_\mathrm{s}(\mathbf{x}) \equiv \hat{\mathbf{j}}(\mathbf{x})p_\mathrm{s}(\mathbf{x})$ (note that $\hat{\mathbf{j}}^g(\mathbf{x})p_\mathrm{s}(\mathbf{x}) = 0$). Moreover, note that the steady-state two-point density $P_\mathbf{y}(\mathbf{x},t) \equiv G(\mathbf{x},t|\mathbf{y})p_\mathrm{s}(\mathbf{y})$ also satisfies the same Fokker-Planck equation as $G(\mathbf{x},t|\mathbf{y})$.

Finally, if the process is irreversible, i.e. $\mathbf{F}^\mathrm{irrev}(\mathbf{x}) \neq \mathbf{0}$ the steady state is dissipative with an average total entropy production rate $\dot{\Sigma}$ given by [21, 68]

$$\begin{aligned} \dot{\Sigma} &= \int d\mathbf{x}\mathbf{F}^\mathrm{irrev}(\mathbf{x})\cdot\mathbf{D}^{-1}(\mathbf{x})\mathbf{F}^\mathrm{irrev}(\mathbf{x})p_\mathrm{s}(\mathbf{x}) \\ &= \int d\mathbf{x}\frac{\mathbf{j}_\mathrm{s}^T(\mathbf{x})}{p_\mathrm{s}(\mathbf{x})}\mathbf{D}^{-1}(\mathbf{x})\mathbf{j}_\mathrm{s}(\mathbf{x}), \end{aligned} \tag{10}$$

which can be obtained as the mean value of a sum over steady-state expectations of the respective i-th component of $\overline{\mathbf{J}_{\mathbf{x}}^{U_i}}(t)$ in Eq. (1) with $U_i = (\mathbf{F}^{\rm irrev}(\mathbf{x})^T\mathbf{D}^{-1}(\mathbf{x}))_i$.

Note that by adopting the Itô or Stratonovich conventions instead of the anti-Itô convention in Eq. (4) one obtains a different Fokker-Planck equation with a different steady-state density. In particular, $L^{\rm Ito}(\mathbf{x}) = -\nabla_{\mathbf{x}}\cdot\mathbf{F}(\mathbf{x}) + \sum_{i,j=1}^{d}\partial_i\partial_j D_{ij}(\mathbf{x})$ and $L^{\rm Strato}(\mathbf{x}) = L(\mathbf{x})/2 + L^{\rm Ito}(\mathbf{x})/2 = -\nabla_{\mathbf{x}}\cdot\mathbf{F}(\mathbf{x}) + \sum_{i,j=1}^{d}\partial_i\sqrt{D_{ij}(\mathbf{x})}\partial_j\sqrt{D_{ij}(\mathbf{x})}$ and the respective steady-state densities $p_{\rm s}^{\rm Ito}(\mathbf{x})$ and $p_{\rm s}^{\rm Strato}(\mathbf{x})$ depend explicitly on $\mathbf{D}(\mathbf{x})$ and are therefore in general not thermodynamically consistent since the steady state deviates from Gibbs-Boltzmann statistics (e.g. in dimension one we have $p_{\rm s}^{\rm Ito}(x) \propto \exp[-\phi(x)]/D(x)$ and $p_{\rm s}^{\rm Strato}(x) \propto \exp[-\phi(x)]/\sqrt{D(x)}$, respectively, where the deviation from $\exp[-\phi(x)]$ cannot be absorbed in the normalization if $D(x)$ depends on x).

III. GENERALIZED TIME-REVERSAL SYMMETRY

It will later prove useful to take into account a form of generalized time-reversal symmetry obeyed by Eq. (4) called "continuous time reversal" or "dual-reversal symmetry" [55, 69]. Analogous generalized symmetries were also found in deterministic systems (see e.g. [70]). Generalized time-reversal symmetry relates forward dynamics in non-equilibrium steady states to time-reversed dynamics in an ensemble with inverted irreversible steady-state current, i.e. in an ensemble with $\mathbf{F}^{\rm irrev} \to -\mathbf{F}^{\rm irrev}$ or equivalently $\mathbf{j}_{\rm s} \to -\mathbf{j}_{\rm s}$. The dual-reversal symmetry for the two-point probability densities states that

$$G(\mathbf{x},t|\mathbf{y})p_{\rm s}(\mathbf{y}) = G^{-\mathbf{j}_{\rm s}}(\mathbf{y},t|\mathbf{x})p_{\rm s}(\mathbf{x}), \tag{11}$$

or equivalently $G^{-\mathbf{j}_{\rm s}}(\mathbf{x},t|\mathbf{y})p_{\rm s}(\mathbf{y}) = G(\mathbf{y},t|\mathbf{x})p_{\rm s}(\mathbf{x})$ where $G^{-\mathbf{j}_{\rm s}}(\mathbf{y},t|\mathbf{x})$ is the conditional probability density of the process with drift $\mathbf{F}^{-\mathbf{j}_{\rm s}}(\mathbf{x}) \equiv \mathbf{F}^{\rm rev}(\mathbf{x}) - \mathbf{F}^{\rm irrev}(\mathbf{x})$ instead of $\mathbf{F}(\mathbf{x}) = \mathbf{F}^{\rm rev}(\mathbf{x}) + \mathbf{F}^{\rm irrev}(\mathbf{x})$. At equilibrium, i.e. $\mathbf{j}_{\rm s}(\mathbf{x}) = \mathbf{0}$ (for all $\mathbf{x}$), this symmetry simplifies to the well known time-reversal symmetry called "detailed balance" condition for two-point densities. We here provide an original and intuitive proof of Eq. (11) that proceeds entirely in continuous space and time, based on the decomposition of currents Eq. (9). The Fokker-Planck operator $L(\mathbf{x}) = -\nabla_{\mathbf{x}}\cdot\hat{\mathbf{j}}_{\mathbf{x}}$, using the decomposition Eq. (9) and multiplying by $p_{\rm s}$ from the right side, reads

$$L(\mathbf{x})p_{\rm s}(\mathbf{x}) = -\nabla_{\mathbf{x}}\cdot\mathbf{j}_{\rm s}(\mathbf{x}) + \nabla_{\mathbf{x}}^T p_{\rm s}(\mathbf{x})\mathbf{D}(\mathbf{x})\nabla_{\mathbf{x}}. \tag{12}$$

Taking the adjoint gives (since $\mathbf{D} = \mathbf{D}^T$)

$$\begin{aligned} p_{\rm s}(\mathbf{x})L^\dagger(\mathbf{x}) &= [L(\mathbf{x})p_{\rm s}(\mathbf{x})]^\dagger \\ &= \mathbf{j}_{\rm s}(\mathbf{x})\cdot\nabla_{\mathbf{x}} + \nabla_{\mathbf{x}}^T p_{\rm s}(\mathbf{x})\mathbf{D}(\mathbf{x})\nabla_{\mathbf{x}}. \end{aligned} \tag{13}$$

Since for the steady state density $Lp_{\rm s} = 0$, $\mathbf{j}_{\rm s}$ is divergence free $\{\nabla_{\mathbf{x}}\cdot\mathbf{j}_{\rm s}(\mathbf{x})\} = 0$ and we have $\nabla_{\mathbf{x}}\cdot\mathbf{j}_{\rm s}(\mathbf{x}) = \mathbf{j}_{\rm s}(\mathbf{x})\cdot\nabla_{\mathbf{x}}$. Thus we see the symmetry under inversion $\mathbf{j}_{\rm s} \to -\mathbf{j}_{\rm s}$

$$p_{\rm s}(\mathbf{x})L^\dagger(\mathbf{x}) = L^{-\mathbf{j}_{\rm s}}(\mathbf{x})p_{\rm s}(\mathbf{x}). \tag{14}$$

Under detailed balance $\mathbf{j}_{\rm s} = \mathbf{0}$, i.e. $L^{-\mathbf{j}_{\rm s}} = L$, and $p_{\rm s}(\mathbf{x})L^\dagger(\mathbf{x}) = L(\mathbf{x})p_{\rm s}(\mathbf{x})$ which implies the time-reversal symmetry $G(\mathbf{x},t|\mathbf{y})p_{\rm s}(\mathbf{y}) = G(\mathbf{y},t|\mathbf{x})p_{\rm s}(\mathbf{x})$ [59, 63, 71]. Eq. (14) implies for all integers $n \geq 1$ that $p_{\rm s}(\mathbf{x})[L^\dagger(\mathbf{x})]^n = [L(\mathbf{x})^{-\mathbf{j}_{\rm s}}]^n(\mathbf{x})p_{\rm s}(\mathbf{x})$, and consequently for all $t \geq 0$ that $p_{\rm s}(\mathbf{x})\exp[L^\dagger(\mathbf{x})t] = \exp[L^{-\mathbf{j}_{\rm s}}(\mathbf{x})t]p_{\rm s}(\mathbf{x})$. Applying this operator equation to the initial condition $\delta(\mathbf{y}-\mathbf{x})$ and using $p_{\rm s}(\mathbf{x})\delta(\mathbf{y}-\mathbf{x}) = p_{\rm s}(\mathbf{y})\delta(\mathbf{y}-\mathbf{x})$ as well as that $L^\dagger$ propagates the initial condition as $G(\mathbf{y},t|\mathbf{x}) = \exp[L^\dagger(\mathbf{x})t]\delta(\mathbf{y}-\mathbf{x})$ while $L^{-\mathbf{j}_{\rm s}}$ propagates the final point in the ensemble with $\mathbf{j}_{\rm s}$ inverted $G^{-\mathbf{j}_{\rm s}}(\mathbf{x},t|\mathbf{y}) = \exp[L^{-\mathbf{j}_{\rm s}}(\mathbf{x})t]\delta(\mathbf{y}-\mathbf{x})$, we obtain the dual reversal symmetry in Eq. (11). This generalized time-reversal symmetry relates the dynamics in the time-reversed ensemble to the propagation in the ensemble with reversed current, or equivalently, the forward dynamics to the propagation with concurrent time and $\mathbf{j}_{\rm s}$-reversal. While at equilibrium (i.e. under detailed balance, $\mathbf{j}_{\rm s} = \mathbf{0}$) the forward dynamics is indistinguishable from the time-reversed dynamics, the statement Eq. (11) (if generalized to all paths (see e.g. [55]) means that forward dynamics (with $\mathbf{j}_{\rm s}$) is indistinguishable from backwards/time-reversed dynamics with reversed $\mathbf{j}_{\rm s} \to -\mathbf{j}_{\rm s}$ (i.e. $\mathbf{j}_{\rm s}(\mathbf{x}) \to -\mathbf{j}_{\rm s}(\mathbf{x})$ at all $\mathbf{x}$). We will later use this dual-reversal symmetry to understand the fluctuations of observables that involve (time-integrated) currents in non-equilibrium steady states.

IV. DERIVATION OF THE MAIN RESULTS, INITIAL- AND FINAL-POINT CURRENTS AND THEIR APPLICATION TO DENSITY-CURRENT CORRELATIONS

A. Mean empirical density and current

Although the time-averaged density and current defined in Eq. (1) are functionals with complicated statistics, their mean values can be readily computed. Throughout the paper we will assume steady-state initial conditions, i.e. initial conditions drawn from $p_{\rm s}(\mathbf{x}')$, denoted by $\langle\cdot\rangle_{\rm s}$. This renders mean values time-independent and we have (see also [6])

$$\begin{aligned} \left\langle\overline{\rho_{\mathbf{x}}^U}(t)\right\rangle_{\rm s} &= \frac{1}{t}\int_0^t d\tau\,\langle U_{\mathbf{x}}^h(\mathbf{x}_\tau)\rangle_{\rm s} \\ &= \frac{1}{t}\int_0^t d\tau\int d\mathbf{z}U_{\mathbf{x}}^h(\mathbf{z})p_{\rm s}(\mathbf{z}) \\ &= \int d\mathbf{z}U_{\mathbf{x}}^h(\mathbf{z})p_{\rm s}(\mathbf{z}), \end{aligned} \tag{15}$$

and by rewriting the Stratonovich-integration $\circ d\mathbf{x}_\tau$ in terms of Itô integration as $U_{\mathbf{x}}^h(\mathbf{x}_\tau)\circ d\mathbf{x}_\tau = U_{\mathbf{x}}^h(\mathbf{x}_\tau)d\mathbf{x}_\tau +$

$\frac{1}{2}dU^h_{\mathbf{x}}(\mathbf{x}_\tau)d\mathbf{x}_\tau$, where $d\mathbf{x}_\tau d\mathbf{x}_\tau^T/2 = \mathbf{D}(\mathbf{x}_\tau)d\tau$ and thus $dU^h_{\mathbf{x}}(\mathbf{x}_\tau)d\mathbf{x}_\tau/2 = \mathbf{D}(\mathbf{x}_\tau)\{\nabla U^h_{\mathbf{x}}\}(\mathbf{x}_\tau)d\tau$,

$$\begin{aligned}\left\langle \overline{\mathbf{J}^U_{\mathbf{x}}}(t)\right\rangle_{\mathrm{s}} &= \frac{1}{t}\int_0^t \left\langle U^h_{\mathbf{x}}(\mathbf{x}_\tau)\circ d\mathbf{x}_\tau\right\rangle_{\mathrm{s}} \\ &= \frac{1}{t}\int_{\tau=0}^{\tau=t}\left\langle U^h_{\mathbf{x}}(\mathbf{x}_\tau)d\mathbf{x}_\tau\right\rangle_{\mathrm{s}} + \frac{1}{t}\int_{\tau=0}^{\tau=t}\frac{1}{2}\left\langle dU^h_{\mathbf{x}}(\mathbf{x}_\tau)d\mathbf{x}_\tau\right\rangle_{\mathrm{s}} \\ &= \frac{1}{t}\int_0^t d\tau\int d\mathbf{z}p_{\mathrm{s}}(\mathbf{z})\big[U^h_{\mathbf{x}}(\mathbf{z})\mathbf{F}(\mathbf{z}) + \left\{\nabla^T_{\mathbf{z}}\mathbf{D}(\mathbf{z})\right\}U^h_{\mathbf{x}}(\mathbf{z}) \\ &+ \mathbf{D}(\mathbf{z})\left\{\nabla_{\mathbf{z}}U^h_{\mathbf{x}}(\mathbf{z})\right\}\big] + \frac{1}{t}\int_{\tau=0}^{\tau=t}\left\langle U^h_{\mathbf{x}}(\mathbf{x}_\tau)\sqrt{2\mathbf{D}(\mathbf{x}_\tau)}d\mathbf{W}_\tau\right\rangle_{\mathrm{s}}.\end{aligned} \tag{16}$$

Note that the mean value involving $d\mathbf{W}_\tau$ vanishes since this Itô-noise increment has zero mean and is uncorrelated with functions of $\mathbf{x}_\tau$, i.e. $\langle f(\mathbf{x}_\tau)d\mathbf{W}_\tau\rangle = \langle f(\mathbf{x}_\tau)\rangle\langle d\mathbf{W}_\tau\rangle = 0$. Integrating by parts and using that $\mathbf{D}(\mathbf{z}) = \mathbf{D}^T(\mathbf{z})$ is symmetric we get

$$\begin{aligned}\left\langle \overline{\mathbf{J}^U_{\mathbf{x}}}(t)\right\rangle_{\mathrm{s}} &= \int d\mathbf{z}p_{\mathrm{s}}(\mathbf{z})\left[U^h_{\mathbf{x}}(\mathbf{z})\mathbf{F}(\mathbf{z}) + \nabla^T_{\mathbf{z}}\mathbf{D}(\mathbf{z})U^h_{\mathbf{x}}(\mathbf{z})\right] \\ &= \int d\mathbf{z}U^h_{\mathbf{x}}(\mathbf{z})\left[\mathbf{F}(\mathbf{z}) - \mathbf{D}(\mathbf{z})\nabla_{\mathbf{z}}\right]p_{\mathrm{s}}(\mathbf{z}) \\ &= \int d\mathbf{z}U^h_{\mathbf{x}}(\mathbf{z})\hat{\mathbf{j}}_{\mathbf{z}}p_{\mathrm{s}}(\mathbf{z}) = \int d\mathbf{z}U^h_{\mathbf{x}}(\mathbf{z})\mathbf{j}_{\mathrm{s}}(\mathbf{z}).\end{aligned} \tag{17}$$

Note that if we had defined Eq. (1) with an Itô integral instead of the Stratonovich, we would miss the $\mathbf{D}(\mathbf{z})\nabla_{\mathbf{z}}$-term and would *not* get $\hat{\mathbf{j}}_{\mathbf{z}}$ and thus $\mathbf{j}_{\mathrm{s}}$, not even for additive noise. The Stratonovich integral is therefore required for consistency.

The interpretation of the steady-state mean values in Eqs. (15) and (17) is immediate — the mean time-averaged density and current are (at least for positive normalized windows) the steady-state density p_{s} and current $\mathbf{j}_{\mathrm{s}}$ averaged over the coarse-graining window function $U^h_{\mathbf{x}}$.

B. (Co)variances of empirical density and current

Since fluctuations [5, 15, 34, 50–55] (and correlations [56]) play a crucial role in time-average statistical mechanics and stochastic thermodynamics, we discuss (co)variances of coarse-grained time-averaged densities and currents (recall the interpretation of the variance within the "fluctuating histogram" picture in Fig. 1).

To keep the notation tractable we introduce the integral operator

$$\hat{\mathcal{I}}^{t,U}_{\mathbf{xy}}[\,\cdot\,] \equiv \frac{1}{t^2}\int_0^t dt_1\int_{t_1}^t dt_2\int d\mathbf{z}U^h_{\mathbf{x}}(\mathbf{z})\int d\mathbf{z}'U^h_{\mathbf{y}}(\mathbf{z}')[\,\cdot\,], \tag{18}$$

with the convention $\int_{t_1}^t dt_2\delta(t_2-t_1) = 1/2$. Note that other conventions would only change the appearance of intermediate steps but not the final result. We define the two-point steady-state covariance according to [58] as

$$C^{\mathbf{xy}}_{AB}(t) \equiv \langle A_{\mathbf{x}}(t)B_{\mathbf{y}}(t)\rangle_{\mathrm{s}} - \langle A_{\mathbf{x}}(t)\rangle_{\mathrm{s}}\langle B_{\mathbf{y}}(t)\rangle_{\mathrm{s}}\,, \tag{19}$$

where A and B are henceforth either $\overline{\rho^U}$ or $\overline{\mathbf{J}^U}$, respectively. We refer to the case when $A \neq B$ or $\mathbf{x} \neq \mathbf{y}$ as (linear) "correlations" and to the case $A = B$ with $\mathbf{x} = \mathbf{y}$ as "fluctuations" whereby we adopt the convention $\mathrm{var}^{\mathbf{x}}_A(t) \equiv C^{\mathbf{xx}}_{AA}(t)$. Note that for simplicity and enhanced readability we only assume coarse-graining windows $U^h_{\mathbf{x}}$ and $U^h_{\mathbf{y}}$ where only the center points $\mathbf{x},\mathbf{y}$ may differ. All results equivalently hold for window functions whose shape and h differs as well.

We now address correlations $C^{\mathbf{xy}}_{\rho\rho}$ of the coarse-grained time-averaged density at points $\mathbf{x}$ and $\mathbf{y}$, which corresponds to the density variance when $\mathbf{x} = \mathbf{y}$. To do so, first consider the (mixed) second moment

$$\left\langle \overline{\rho^U_{\mathbf{x}}}(t)\overline{\rho^U_{\mathbf{y}}}(t)\right\rangle_{\mathrm{s}} = \int_0^t d\tau\int_0^t d\tau'\left\langle U^h_{\mathbf{x}}(\mathbf{x}_\tau)U^h_{\mathbf{y}}(\mathbf{x}'_\tau)\right\rangle_{\mathrm{s}}. \tag{20}$$

The expectation value corresponds to an integration over the two-point probability density to have $\mathbf{x}_\tau = \mathbf{z}$ and $\mathbf{x}_{\tau'} = \mathbf{z}'$ given by the two-point function $P_{\mathbf{z}}(\mathbf{z}',\tau'-\tau) \equiv G(\mathbf{z}',\tau'-\tau|\mathbf{z})p_{\mathrm{s}}(\mathbf{z})$ for $\tau' > \tau$ and $P_{\mathbf{z}'}(\mathbf{z},\tau-\tau')$ for $\tau' < \tau$. We relabel the times τ,τ' as $t_1 < t_2$ and use the integral operator in Eq. (18) to obtain

$$\left\langle \overline{\rho^U_{\mathbf{x}}}(t)\overline{\rho^U_{\mathbf{y}}}(t)\right\rangle_{\mathrm{s}} = \hat{\mathcal{I}}^{t,U}_{\mathbf{xy}}\left[P_{\mathbf{z}}(\mathbf{z}',t_2-t_1) + P_{\mathbf{z}}(\mathbf{z}',t_2-t_1)\right]. \tag{21}$$

Since the argument only depends on time differences $t' = t_2 - t_1 \geq 0$ the integral operator Eq. (18) simplifies to

$$\hat{\mathcal{I}}^{t,U}_{\mathbf{xy}}[\,\cdot\,] \equiv \frac{1}{t}\int_0^t dt'\left(1-\frac{t'}{t}\right)\int d\mathbf{z}U^h_{\mathbf{x}}(\mathbf{z})\int d\mathbf{z}'U^h_{\mathbf{y}}(\mathbf{z}')[\,\cdot\,]. \tag{22}$$

To obtain the correlation we subtract the mean values (see Eq. (15)) which (noting that $(1/t)\int_0^t dt'(1-t'/t) = 1/2$) gives

$$C^{\mathbf{xy}}_{\rho\rho}(t) = \hat{\mathcal{I}}^{t,U}_{\mathbf{xy}}\left[P_{\mathbf{z}}(\mathbf{z}',t') + P_{\mathbf{z}'}(\mathbf{z},t') - 2p_{\mathrm{s}}(\mathbf{z})p_{\mathrm{s}}(\mathbf{z}')\right], \tag{23}$$

which has been derived before [51, 72]. Eq. (23) simplifies further for $\mathbf{x} = \mathbf{y}$ as well as under detailed balance and is also symmetric under $\mathbf{j}_{\mathrm{s}} \to -\mathbf{j}_{\mathrm{s}}$, all of which will be discussed in Sec. VI.

The interpretation of Eq. (23) (see also [51]) is that all paths from $\mathbf{z}$ to $\mathbf{z}'$ (i.e. from $U^h_{\mathbf{x}}$ to $U^h_{\mathbf{y}}$) and vice versa from $\mathbf{z}'$ to $\mathbf{z}$, in time $t' = t_2 - t_1$ contribute according to their correlation to $C^{\mathbf{xy}}_{\rho\rho}(t)$. These contributions are integrated over all possible time differences and pairs of points within $U^h_{\mathbf{x}}$ and $U^h_{\mathbf{y}}$, respectively.

We now explore the important effect of coarse graining over the windows $U^h_{\mathbf{x}}$ for the inference of $p_{\mathrm{s}}(\mathbf{x})$ from noisy individual trajectories. If one wants to reliably infer the

(coarse-grained) steady-state density from $\overline{\rho^U_{\mathbf{x}}}(t)$ the relative error $\mathrm{var}_\rho/\langle\overline{\rho^U_{\mathbf{x}}}(t)\rangle^2$ should be small. We have shown that $\lim_{h\to 0}\mathrm{var}_\rho/\langle\overline{\rho^U_{\mathbf{x}}}(t)\rangle^2=\infty$ [58] and Fig. 3 (blue line) demonstrates that $\mathrm{var}_\rho/\langle\overline{\rho^U_{\mathbf{x}}}(t)\rangle^2$ decreases with increasing h. However, such a decrease does not guarantee an improved inference. Namely, as $h\to\infty$ the time to spent in the region around $\mathbf{x}$ tends to t and $U^h_{\mathbf{x}}$ becomes constant on a large region and hence $\overline{\rho^U_{\mathbf{x}}}(t)\to U^h_{\mathbf{x}}(\mathbf{x})$ which contains no information about $p_{\mathrm{s}}(\mathbf{x})$. Therefore, to reliably infer that $\overline{\rho^U_{\mathbf{x}}}$ significantly deviates from $U^h_{\mathbf{x}}(\mathbf{x})$ we must also consider the relative error of $[\overline{\rho^U_{\mathbf{x}}}-U^h_{\mathbf{x}}(\mathbf{x})]$ depicted in Fig. 3 (orange line). There exists an "optimal coarse graining" where the uncertainty of simultaneously inferring $\overline{\rho^U_{\mathbf{x}}}$ and $\overline{\rho^U_{\mathbf{x}}}-U^h_{\mathbf{x}}(\mathbf{x})$ is minimal (minimum of the solid lines in Fig. 3) which represents the most reliable and informative estimate of $\overline{\rho^U_{\mathbf{x}}}$. In Sec. V we will turn to an analogous "optimal coarse graining" with respect to current variances and a system's dissipation.

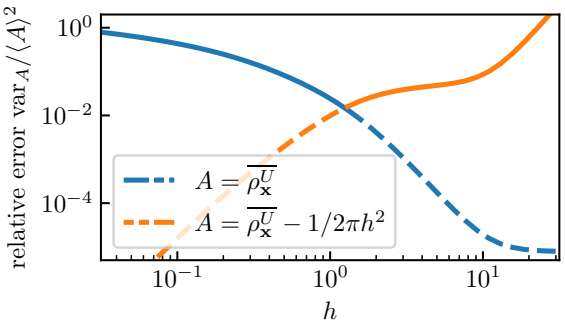

FIG. 3. Relative error of $\overline{\rho^U_{\mathbf{x}}}(t)$ (blue line) compared to the relative error of $[\overline{\rho^U_{\mathbf{x}}}(t)-U^h_{\mathbf{x}}(\mathbf{x})]$ (orange line) as a function of the coarsening scale h for the rotational flow Eq. (2) with $\Omega=3$ for time $t=10$ with a Gaussian window function Eq. (3) around $\mathbf{x}=(1,0)^T$ with width h, i.e. $U^h_{\mathbf{x}}(\mathbf{x})=(2\pi h^2)^{-1}$. The intersection point of blue and orange lines at $h\approx 1.3$ yields an "optimal coarse graining" where the maximum of the two lines (solid line) is minimal, whereas the maximum of the relative errors diverges as $h\to\infty$ since $\langle A\rangle_{\mathrm{s}}\to 0$ and diverges logarithmically for $h\to 0$ [58].

We now consider coarse-grained time-averaged currents. To compute the correlation of the current at a point $\mathbf{x}$ and the density at $\mathbf{y}$ we need to consider

$$\left\langle\overline{\mathbf{J}^U_{\mathbf{x}}}(t)\overline{\rho^U_{\mathbf{y}}}(t)\right\rangle_{\mathrm{s}}=\int_0^t d\tau\int_{\tau'=0}^{\tau'=t}\left\langle U^h_{\mathbf{x}}(\mathbf{x}_\tau)U^h_{\mathbf{y}}(\mathbf{x}'_\tau)\circ d\mathbf{x}_{\tau'}\right\rangle_{\mathrm{s}}. \tag{24}$$

Relabeling with $t_1\le t_2$, introducing the notation

$$\langle\cdots\rangle^{\mathbf{x}_{t_1}=\mathbf{z}}_{\mathbf{x}_{t_2}=\mathbf{z}'}\equiv\langle\delta(\mathbf{x}_{t_1}-\mathbf{z})\delta(\mathbf{x}_{t_2}-\mathbf{z}')\cdots\rangle_{\mathrm{s}}, \tag{25}$$

and considering the Stratonovich increments

$$\circ d\mathbf{x}_\tau\equiv\mathbf{x}_{\tau+d\tau/2}-\mathbf{x}_{\tau-d\tau/2}, \tag{26}$$

and subtracting the mean values (15) and (17), we can write the correlation as

$$\mathbf{C}^{\mathbf{xy}}_{\mathbf{J}_\rho}(t)=\hat{\mathcal{I}}^{t,U}_{\mathbf{xy}}\left[\frac{\langle\circ d\mathbf{x}_{t_1}\rangle^{\mathbf{x}_{t_2}=\mathbf{z}'}_{\mathbf{x}_{t_1}=\mathbf{z}}}{dt_1}+\frac{\langle\circ d\mathbf{x}_{t_2}\rangle^{\mathbf{x}_{t_2}=\mathbf{z}}_{\mathbf{x}_{t_1}=\mathbf{z}'}}{dt_2}-2\mathbf{j}_{\mathrm{s}}(\mathbf{z})p_{\mathrm{s}}(\mathbf{z}')\right]. \tag{27}$$

Eq. (27) is harder to compute and more difficult to interpret as compared to $C^{\mathbf{xy}}_{\rho\rho}(t)$ (see Eq. (23)). The quantities involving Stratonovich increments contain increments at times t_1 or $t_2>t_1$. The increments are conditioned on initial and final points $\mathbf{z},\mathbf{z}'$ where $\mathbf{z}$ always denotes the point where the increment occurs. Via the integral operator in Eq. (18) or (22) the $\mathbf{z}$ variable is integrated over $U^h_{\mathbf{x}}(\mathbf{z})$, i.e. in $\mathbf{C}^{\mathbf{xy}}_{\mathbf{J}_\rho}(t)$ the variable $\mathbf{z}$ corresponds to the position at which the (coarse-grained) current is evaluated. That means that correlations of a current in a window at $\mathbf{x}$ and density in a window at $\mathbf{y}$ depend on initial-point increments at time t_1 at $\mathbf{x}$ conditioned on reaching point in a window at $\mathbf{y}$ at t_2, and on final-point increments at time t_2 in a window at $\mathbf{x}$ conditioned on starting in a window at point $\mathbf{y}$ at t_1. We define the increments divided by dt_i to be the "initial- and final-point currents",

$$\mathbf{j}_{\mathrm{in}}(\mathbf{z}',t_2-t_1;\mathbf{z})\equiv\frac{\langle\circ d\mathbf{x}_{t_1}\rangle^{\mathbf{x}_{t_2}=\mathbf{z}'}_{\mathbf{x}_{t_1}=\mathbf{z}}}{dt_1}$$
$$\mathbf{j}_{\mathrm{fi}}(\mathbf{z},t_2-t_1;\mathbf{z}')\equiv\frac{\langle\circ d\mathbf{x}_{t_2}\rangle^{\mathbf{x}_{t_2}=\mathbf{z}}_{\mathbf{x}_{t_1}=\mathbf{z}'}}{dt_2}. \tag{28}$$

In order to understand the correlation in Eq. (27) we must therefore understand initial- and final-point currents. This is *a priori* not easy, since initial-point currents involve both, spatial increments at t_1 and probabilities of reaching a final point at time $t_2>t_1$, which involves non-trivial correlations — a given displacement affects (and thus correlates with) the probability to reach the final point. We will derive a statement ("Lemma") in the next subsection that solves all mathematical difficulties related to this issue. Then we will make intuitive sense of the result by exploiting the dual-reversal symmetry in Eq. (11).

Before doing so, we also consider the scalar current-current covariance $C^{\mathbf{xy}}_{\mathbf{J}\cdot\mathbf{J}}(t)$ (note that the complete fluctuations and correlations of $\overline{\mathbf{J}^U_{\mathbf{x}}}(t)$ are characterized by the $d\times d$ covariance matrix with elements $(\mathbf{C}^{\mathbf{xy}}_{\mathbf{JJ}}(t))_{ik}=C^{\mathbf{xy}}_{\mathbf{J}_i\mathbf{J}_k}(t)$; here we focus on the scalar case $C^{\mathbf{xy}}_{\mathbf{J}\cdot\mathbf{J}}(t)\equiv\mathrm{Tr}\mathbf{C}^{\mathbf{xy}}_{\mathbf{JJ}}(t)$). Notably, almost all results remain completely equivalent for other elements of the covariance matrix, scalar products simply have a slightly more intuitive geometrical interpretation and notation. Writing down the definition and using the notations as in the steps towards

Eq. (27) we immediately arrive at

$$C^{\mathbf{xy}}_{\mathbf{J}\cdot\mathbf{J}}(t) = \hat{\mathcal{I}}^{t,U}_{\mathbf{xy}}\Bigg[\frac{\langle \circ d\mathbf{x}_{t_1}\cdot\circ d\mathbf{x}_{t_2}\rangle^{\mathbf{x}_{t_2}=\mathbf{z}'}_{\mathbf{x}_{t_1}=\mathbf{z}}}{dt_1 dt_2} + \frac{\langle \circ d\mathbf{x}_{t_1}\cdot\circ d\mathbf{x}_{t_2}\rangle^{\mathbf{x}_{t_2}=\mathbf{z}}_{\mathbf{x}_{t_1}=\mathbf{z}'}}{dt_1 dt_2} - 2\mathbf{j}_{\mathrm{s}}(\mathbf{z})\cdot\mathbf{j}_{\mathrm{s}}(\mathbf{z}')\Bigg], \tag{29}$$

which is similar to the correlation in Eq. (27) but involves an average over scalar products of initial- and final-point increments along individual trajectories "pinned" at initial- and end-points. We will return to Eq. (29) and solve for these increments in Subsec. IV F upon having explained the density-current correlation.

C. Lemma

To be able to treat expressions involving the increments correlated with future positions, we need a technical lemma that will turn out to be very powerful and central to all calculations. Consider an Itô noise increment $\sqrt{2\mathbf{D}(\mathbf{x}_\tau)}d\mathbf{W}_\tau$ (or equivalently $\boldsymbol{\sigma}(\mathbf{x}_\tau)d\mathbf{W}_\tau$) with $d\mathbf{W}_\tau = \mathbf{W}_{\tau+d\tau} - \mathbf{W}_\tau$. In the following we will need to compute the expected values involving expressions like

$$\star = \left\langle \left[\sqrt{2\mathbf{D}(\mathbf{x}_\tau)}d\mathbf{W}_\tau\right]_k U(\mathbf{x}_\tau)V(\mathbf{x}_{\tau'})\right\rangle_{\mathrm{s}}, \tag{30}$$

where $U(\mathbf{x}')$ and $V(\mathbf{x}')$ are arbitrary differentiable, square integrable functions, the subscript k denotes the k-th component, and the subscript s denotes that the process evolves from $p_{\mathrm{s}}(\mathbf{x}')$. Correlations of $d\mathbf{W}_\tau = \mathbf{W}_{\tau+d\tau} - \mathbf{W}_\tau$ with any function of $\mathbf{x}_{\tau'}$ at a time $\tau' \leq \tau$ vanish by construction of the Wiener process (it has nominally independent increments). However, correlations with functions at $\tau' > \tau$ are nontrivial.

Note that given an initial point $\mathbf{x}_0 = \mathbf{z}$ and setting $\sqrt{2\mathbf{D}(\mathbf{z})}d\mathbf{W_0} = \boldsymbol{\varepsilon}$, the Itô/Langevin Eq. (5) predicts a displacement $d\mathbf{x}_0(\mathbf{z},\boldsymbol{\varepsilon}) = [\mathbf{F}(\mathbf{z}) + \nabla_{\mathbf{z}}^T\mathbf{D}(\mathbf{z})]dt' + \boldsymbol{\varepsilon}$. With this we can write the expectation in Eq. (30) for $\tau = 0 < t' = \tau'$ as ε_k integrated over the probability to be at points $\mathbf{z}, \mathbf{z} + d\mathbf{x}_0(\mathbf{z},\boldsymbol{\varepsilon}), \mathbf{z}'$ at times $0, dt', t'$, i.e.

$$\star = \int d\mathbf{z}\int d\mathbf{z}' U(\mathbf{z})V(\mathbf{z}')\times \int d\boldsymbol{\varepsilon}\,\mathbb{P}(\boldsymbol{\varepsilon})\varepsilon_k G(\mathbf{z}', t'-dt'|\mathbf{z}+d\mathbf{x}_0(\mathbf{z},\boldsymbol{\varepsilon}))p_{\mathrm{s}}(\mathbf{z}), \tag{31}$$

where the probability $\mathbb{P}(\boldsymbol{\varepsilon})$ of $\sqrt{2\mathbf{D}(\mathbf{z})}d\mathbf{W_0} = \boldsymbol{\varepsilon}$ is given by a Gaussian distribution with zero mean and covariance matrix $2\mathbf{D}(\mathbf{z})dt'$. Since this distribution is symmetric around $\mathbf{0}$, only terms with even powers of the components of $\boldsymbol{\varepsilon}$ survive the $\mathbb{P}(\boldsymbol{\varepsilon})$-integration. Noting that for $dt' \to 0$ we have $G(\mathbf{z}', t'-dt'|\mathbf{z}+d\mathbf{x}_0(\mathbf{z},\boldsymbol{\varepsilon})) \to [1 + d\mathbf{x}_0(\mathbf{z},\boldsymbol{\varepsilon})\cdot\nabla_{\mathbf{z}}]G(\mathbf{z}', t'|\mathbf{z})$, we see that the only even power of the components of $\boldsymbol{\varepsilon}$ in $\varepsilon_k G(\dots)$ gives

$$\star = \int d\mathbf{z}\int d\mathbf{z}' U(\mathbf{z})p_{\mathrm{s}}(\mathbf{z})V(\mathbf{z}')\times \int d\boldsymbol{\varepsilon}\,\mathbb{P}(\boldsymbol{\varepsilon})\varepsilon_k\boldsymbol{\varepsilon}\cdot\nabla_{\mathbf{z}}G(\mathbf{z}', t'|\mathbf{z}), \tag{32}$$

which using $\int d\boldsymbol{\varepsilon}\mathbb{P}(\boldsymbol{\varepsilon})\varepsilon_k\varepsilon_j = 2D_{kj}(\mathbf{z})dt'$ yields the result

$$\star = \int d\mathbf{z}\int d\mathbf{z}' U(\mathbf{z})p_{\mathrm{s}}(\mathbf{z})V(\mathbf{z}')\left[2\mathbf{D}(\mathbf{z})\nabla_{\mathbf{z}}G(\mathbf{z}', t'|\mathbf{z})\right]_k dt'. \tag{33}$$

Rewritten terms of $P_{\mathbf{z}}(\mathbf{z}', t') \equiv G(\mathbf{z}', t'|\mathbf{z})p_{\mathrm{s}}(\mathbf{z})$ and $\hat{\mathbf{j}}^g_{\mathbf{z}} \equiv -p_{\mathrm{s}}(\mathbf{z})\mathbf{D}(\mathbf{z})\nabla_{\mathbf{z}}p_{\mathrm{s}}^{-1}(\mathbf{z})$ we have $\hat{\mathbf{j}}^g_{\mathbf{z}}P_{\mathbf{z}}(\mathbf{z}', t') = -p_{\mathrm{s}}(\mathbf{z})\mathbf{D}(\mathbf{z})\nabla_{\mathbf{z}}G(\mathbf{z}', t'|\mathbf{z})$, and thus

$$\star = -2\int d\mathbf{z}\int d\mathbf{z}' U(\mathbf{z})V(\mathbf{z}')\left[\hat{\mathbf{j}}^g_{\mathbf{z}}\right]_k P_{\mathbf{z}}(\mathbf{z}', t')dt'. \tag{34}$$

Motivated by the dual-reversal symmetry and the anticipated applications we define the dual-reversed current operator by inverting $\hat{\mathbf{j}}$ and concurrently inverting $\mathbf{j}_{\mathrm{s}} \to -\mathbf{j}_{\mathrm{s}}$, i.e.

$$\hat{\mathbf{j}}^{\ddagger}_{\mathbf{x}} \equiv -\hat{\mathbf{j}}^{-\mathbf{j}_{\mathrm{s}}}_{\mathbf{x}} = -\left[\hat{\mathbf{j}}^g_{\mathbf{x}} - p_{\mathrm{s}}^{-1}(\mathbf{x})\mathbf{j}_{\mathrm{s}}(\mathbf{x})\right] = p_{\mathrm{s}}(\mathbf{x})\mathbf{D}(\mathbf{x})\nabla_{\mathbf{x}}p_{\mathrm{s}}^{-1}(\mathbf{x}) + p_{\mathrm{s}}^{-1}(\mathbf{x})\mathbf{j}_{\mathrm{s}}(\mathbf{x}). \tag{35}$$

Since $\hat{\mathbf{j}}^{\ddagger}_{\mathbf{z}} - \hat{\mathbf{j}}_{\mathbf{z}} = -2\hat{\mathbf{j}}^g$ we can rewrite Eqs. (33)-(34) as

$$\star = \int d\mathbf{z}\int d\mathbf{z}' U(\mathbf{z})V(\mathbf{z}')\left(\hat{\mathbf{j}}^{\ddagger}_{\mathbf{z}} - \hat{\mathbf{j}}_{\mathbf{z}}\right)_k P_{\mathbf{z}}(\mathbf{z}', t')dt', \tag{36}$$

which will turn out to be the crucial part of the following calculations and will allow for an intuitive interpretation of the results in terms of dual-reversed dynamics.

D. Application of the Lemma to initial- and final-point currents

In order to quantify and understand the density-current correlation expression in Eq. (27), we now turn back to the initial- and final-point currents, recalling the definitions in Eq. (28). These observables characterize the mean initial- and final displacements of "pinned" paths of duration $t_2 - t_1$ conditioned on the respective initial and final points $\mathbf{z}, \mathbf{z}'$ or $\mathbf{z}', \mathbf{z}$. The fact that both are currents in $\mathbf{z}$ justifies the name "initial- and final-point current". Such objects turn out to play a crucial role in the evaluation and understanding of correlations of densities and currents, see Eq. (27). The computation of current variances in fact involves the expectation of scalar products of such displacements (see Eq. (29)), but we first focus on simple displacements.

Final-point currents can be computed by substituting for $\circ d\mathbf{x}_\tau$ and integrating by parts as in Eq. (17),

$$\begin{aligned}\frac{\langle \circ d\mathbf{x}_{t_2}\rangle_{\mathbf{x}_{t_1}=\mathbf{z}'}^{\mathbf{x}_{t_2}=\mathbf{z}}}{dt_2} =& \int d\mathbf{z}_1 \int d\mathbf{z}_2 \delta(\mathbf{z}_1-\mathbf{z}')\delta(\mathbf{z}_2-\mathbf{z})\times \\ & P_{\mathbf{z}_1}(\mathbf{z}_2,t_2-t_1)[\mathbf{F}(\mathbf{z}_2)+\nabla_{\mathbf{z}_2}^T\mathbf{D}(\mathbf{z}_2)] \\ =&[\mathbf{F}(\mathbf{z})-\mathbf{D}(\mathbf{z})\nabla_{\mathbf{z}}]P_{\mathbf{z}'}(\mathbf{z},t_2-t_1) \\ =&\hat{\mathbf{j}}_{\mathbf{z}}P_{\mathbf{z}'}(\mathbf{z},t_2-t_1), \end{aligned} \tag{37}$$

where the Itô term involving $d\mathbf{W}_{t_2}$ vanishes whereas the Stratonovich correction term survives. Therefore, the final-point current is obtained from the two-point density and current operator, both appearing in the Fokker-Planck equation (recall that $(\partial_t+\nabla_{\mathbf{x}}\cdot\hat{\mathbf{j}}_{\mathbf{x}})P_{\mathbf{y}}(\mathbf{x},t)=0$)

$$\mathbf{j}_{\rm fi}(\mathbf{z},t_2-t_1;\mathbf{z}')=\hat{\mathbf{j}}_{\mathbf{z}}P_{\mathbf{z}'}(\mathbf{z},t_2-t_1). \tag{38}$$

For the initial-point current analogous computations yield an Itô increment as a correction

$$\begin{aligned}\mathbf{j}_{\rm in}(\mathbf{z}',t_2-t_1;\mathbf{z}) =& \hat{\mathbf{j}}_{\mathbf{z}}P_{\mathbf{z}}(\mathbf{z}',t_2-t_1) \\ &+\langle\sqrt{2\mathbf{D}(\mathbf{x}_{t_1})}d\mathbf{W}_{t_1}\rangle_{\mathbf{x}_{t_1}=\mathbf{z}}^{\mathbf{x}_{t_2}=\mathbf{z}'}. \end{aligned} \tag{39}$$

Note that the latter Itô increment also appears in the calculations in Eqs. (17) and (37), but its mean vanishes since it involves end-point increments $d\mathbf{W}_{t_2}$ (note t_2 and not t_1), which are by construction uncorrelated with the evolution up to time t_2. The correction term here does *not* vanish since the increment at time t_1 is correlated with the probability to reach $\mathbf{z}'$ at time t_2. Therefore this expectation is non-trivial, but fortunately we solved this problem with the Lemma derived in Eqs. (30)-(36).

When U and V in Eq. (36) tend to a Dirac delta function (which is mathematically not problematic since we later integrate over $\mathbf{z},\mathbf{z}'$) we obtain

$$\langle\sqrt{2\mathbf{D}(\mathbf{x}_{t_1})}d\mathbf{W}_{t_1}\rangle_{\mathbf{x}_{t_1}=\mathbf{z}}^{\mathbf{x}_{t_2}=\mathbf{z}'} = \left(\hat{\mathbf{j}}_{\mathbf{z}}^{\dagger}-\hat{\mathbf{j}}_{\mathbf{z}}\right)P_{\mathbf{z}}(\mathbf{z}',t_2-t_1), \tag{40}$$

which gives, recalling Eq. (35),

$$\mathbf{j}_{\rm in}(\mathbf{z}',t_2-t_1;\mathbf{z})=\hat{\mathbf{j}}_{\mathbf{z}}^{\dagger}P_{\mathbf{z}}(\mathbf{z}',t_2-t_1). \tag{41}$$

Note that $\mathbf{j}_{\rm in}(\mathbf{y},t;\mathbf{x},0)=-\mathbf{j}_{\rm fi}^{-\mathbf{j}_{\rm s}}(\mathbf{x},t;\mathbf{y},0)$ in agreement with dual-reversal symmetry.

To better understand these currents and their symmetry we require some intuition about the generalized time-reversal symmetry (i.e. the dual-reversal symmetry), which we gain on the basis of a simple overdamped shear flow in Fig. 4. Consider an isotropic diffusion with additive noise in a shear flow $d\mathbf{x}_\tau=\mathbf{F}_{\rm sh}(\mathbf{x}_\tau)d\tau+\sqrt{2}d\mathbf{W}_\tau$ with $\mathbf{F}_{\rm sh}((x,y)^T)=(0,2x)^T$ (see gray arrows in Fig. 4a-c). The shear drift is purely irreversible, i.e. $\mathbf{F}_{\rm sh}^{\rm rev}(\mathbf{x}')=\mathbf{0}$. Thus, inverting the irreversible part completely inverts the drift $\mathbf{F}_{\rm sh}^{-\mathbf{j}_{\rm s}}(\mathbf{x}')=-\mathbf{F}_{\rm sh}(\mathbf{x}')$, see blue arrows in Fig. 4a,d. The initial-point current (purple arrow in Fig. 4b) is difficult to understand, since it correlates with the constraint to reach the end point after time t'. In the case of detailed balance, the time-reversal symmetry would allow to obtain this initial-point current as the inverted final-point current (yellow arrow in Fig. 4c). However, since detailed balance is broken by the shear flow this does not suffice. Instead, one has to consider the final-point current for the dynamics with the inverted irreversible drift (blue arrow in Fig. 4d). According to $\mathbf{j}_{\rm in}(\mathbf{y},t;\mathbf{x},0)=-\mathbf{j}_{\rm fi}^{-\mathbf{j}_{\rm s}}(\mathbf{x},t;\mathbf{y},0)$ and as can be seen in Fig. 4a, this allows to obtain the cumbersome initial-point current (yellow) as the inverted final point current (blue).

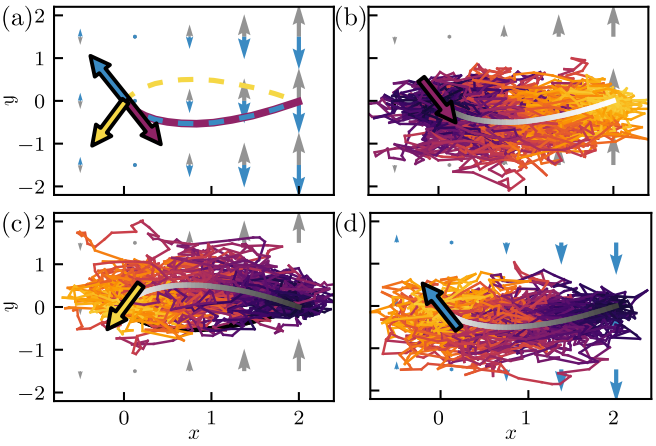

FIG. 4. (a) Shear drift (gray background arrows) and inverted shear drift (blue background arrows) as described in the text, and currents and paths from (b-d) shown in purple, yellow and blue. We see that the purple arrow equals the inverted blue arrow, and the purple line overlaps with the blue dashed line, as implied by Eq. (43). (b) Simulated trajectories in the shear flow (gray background arrows) from $\mathbf{z}=(0,0)^T$ to $\mathbf{z}'=(2,0)^T$ in time $t'=1$ with time always running from dark to bright. The initial-point current, i.e. the initial-point increment averaged over all trajectories, is depicted by the purple arrow and the mean paths (averaged over all trajectories) by the grey curve. (c) As in (b) but from $\mathbf{z}'=(2,0)^T$ to $\mathbf{z}=(0,0)^T$ and final-point current depicted by a yellow arrow. (d) As in (c) but with the inverted shear flow depicted by blue arrows in the background.

In addition to the initial- and final-point currents, we also depict in Fig. 4 the mean "pinned" paths. In Fig. 4a we see that the forward and dual-reversed paths (purple and blue dashed lines) overlap. This can also be seen from the dual-reversal symmetry in Eq. (11).

To prove the equality of mean paths consider $0<\tau<t'$ where $t'=t_2-t_2>0$. The (non-random) point $\boldsymbol{\mu}(\tau)\equiv\langle\mathbf{x}_{t_1+\tau}\rangle_{\mathbf{x}_{t_1}=\mathbf{z}}^{\mathbf{x}_{t_2}=\mathbf{z}'}$ on the mean path $\mathbf{z}\to\mathbf{z}'$ is given by an integral over all possible intermediate points $\boldsymbol{\mu}(\tau)=\mathbf{x}$ weighted by $G(\mathbf{z}',t'-\tau|\mathbf{x})G(\mathbf{x},\tau|\mathbf{z})/G(\mathbf{z}',t'|\mathbf{z})$ (since $\mathbf{x}_\tau$ is a Markov process) which gives the Chapman-

Kolmogorov-like equation

$$G(\mathbf{z}',t'|\mathbf{z})\boldsymbol{\mu}(\tau)=\int d\mathbf{x}G(\mathbf{z}',t'-\tau|\mathbf{x})G(\mathbf{x},\tau|\mathbf{z})\mathbf{x}. \quad (42)$$

The corresponding point on the mean dual-reversed path $\boldsymbol{\mu}^\ddagger(\tau)\equiv\langle\mathbf{x}_{t_2-\tau}^{-\mathbf{j}_\mathrm{s}}\rangle_{\mathbf{x}_{t_1}=\mathbf{z}'}^{\mathbf{x}_{t_2}=\mathbf{z}}$ from $\mathbf{z}'$ to $\mathbf{z}$ with reversed steady-state current $\mathbf{j}_\mathrm{s}\to-\mathbf{j}_\mathrm{s}$ is given by (using three times the dual-reversal in Eq. (11))

$$\begin{aligned}
&G^{-\mathbf{j}_\mathrm{s}}(\mathbf{z},t'|\mathbf{z}')\boldsymbol{\mu}^\ddagger(t'-\tau)\\
&=\int d\mathbf{x}G^{-\mathbf{j}_\mathrm{s}}(\mathbf{z},\tau|\mathbf{x})G^{-\mathbf{j}_\mathrm{s}}(\mathbf{x},t'-\tau|\mathbf{z}')\mathbf{x}\\
&=\int d\mathbf{x}G(\mathbf{x},\tau|\mathbf{z})\frac{p_\mathrm{s}(\mathbf{z})}{p_\mathrm{s}(\mathbf{x})}G(\mathbf{z}',t'-\tau|\mathbf{x})\frac{p_\mathrm{s}(\mathbf{x})}{p_\mathrm{s}(\mathbf{z}')}\mathbf{x}\\
&=\frac{p_\mathrm{s}(\mathbf{z})}{p_\mathrm{s}(\mathbf{z}')}G(\mathbf{z}',t'|\mathbf{z})\boldsymbol{\mu}(\tau)\\
&=G^{-\mathbf{j}_\mathrm{s}}(\mathbf{z},t'|\mathbf{z}')\boldsymbol{\mu}(\tau), \quad (43)
\end{aligned}$$

which implies $\boldsymbol{\mu}(\tau)=\boldsymbol{\mu}^\ddagger(t'-\tau)$ for all $t_1<\tau<t_2$, so the mean paths indeed agree (but run in opposite directions), which completes the proof that the blue and purple paths in Fig. 4a overlap.

E. Current-density correlation

With the definitions (28) and $t'=t_2-t_1>0$ we have (recall the simplification of $\hat{\mathcal{I}}_{\mathbf{xy}}^{t,U}$ in Eq. (22))

$$\mathbf{C}_{\mathbf{J}\rho}^{\mathbf{xy}}(t)=\hat{\mathcal{I}}_{\mathbf{xy}}^{t,U}[\mathbf{j}_\mathrm{fi}(\mathbf{z},t';\mathbf{z}')+\mathbf{j}_\mathrm{in}(\mathbf{z}',t';\mathbf{z})-2\mathbf{j}_\mathrm{s}(\mathbf{z})p_\mathrm{s}(\mathbf{z}')]. \quad (44)$$

As we have shown in Eqs. (38) and (41) the initial- and final-point currents can be expressed in terms of the current operators yielding

$$\mathbf{C}_{\mathbf{J}\rho}^{\mathbf{xy}}(t)=\hat{\mathcal{I}}_{\mathbf{xy}}^{t,U}[\hat{\mathbf{j}}_\mathbf{z}P_{\mathbf{z}'}(\mathbf{z},t')+\hat{\mathbf{j}}_\mathbf{z}^\ddagger P_\mathbf{z}(\mathbf{z}',t')-2\mathbf{j}_\mathrm{s}(\mathbf{z})p_\mathrm{s}(\mathbf{z}')], \quad (45)$$

which allows to explicitly calculate $\mathbf{C}_{\mathbf{J}\rho}^{\mathbf{xy}}(t)$ if $P_{\mathbf{z}'}(\mathbf{z},t')$ is known. An analogous result for the scalar current variance was very recently obtained in [55] but did not establish a connection to current operators and dual-reversal symmetry and did not consider coarse graining nor multi-dimensional continuous-space examples. The current-density correlation $\mathbf{C}_{\mathbf{J}\rho}^{\mathbf{xy}}(t)$ can be interpreted analogous to $\mathbf{C}_{\rho\rho}^{\mathbf{xy}}(t)$ as follows.

All possible paths between points $\mathbf{z},\mathbf{z}'$ in time $0<t'\leq t$ contribute, weighted by their corresponding probability, to this correlation. The difference with respect to density correlations $\mathbf{C}_{\rho\rho}^{\mathbf{xy}}(t)$ is that now currents at position $\mathbf{z}$ are correlated with probabilities to be at the point $\mathbf{z}'$. For paths $\mathbf{z}'\to\mathbf{z}$ the displacement is obtained from the familiar current operator $\mathbf{j}_\mathrm{fi}=\hat{\mathbf{j}}_\mathbf{z}P_{\mathbf{z}'}(\mathbf{z},t')$. Paths from $\mathbf{z}\to\mathbf{z}'$ are mathematically more involved (and somewhat harder to understand), but can be understood intuitively with the dual-reversal symmetry (see also Fig. 4). More precisely, they can be understood and calculated in terms of the dual-reversed current operator $\hat{\mathbf{j}}_\mathbf{z}^\ddagger\equiv-\hat{\mathbf{j}}_\mathbf{z}^{-\mathbf{j}_\mathrm{s}}$.

A direct observation that follows from the result in Eq. (45) is that at equilibrium (i.e. under detailed balance), we have $\mathbf{j}_\mathrm{s}=\mathbf{0}$, $\hat{\mathbf{j}}_\mathbf{z}^\ddagger=-\hat{\mathbf{j}}_\mathbf{z}$ and $P_\mathbf{z}(\mathbf{z}',t')=P_{\mathbf{z}'}(\mathbf{z},t')$ and thus $\mathbf{C}_{\mathbf{J}\rho}^{\mathbf{xy}}(t)=\mathbf{0}$ for all window functions and all points $\mathbf{x},\mathbf{y}$. The correlation $\mathbf{C}_{\mathbf{J}\rho}^{\mathbf{xy}}(t)$ can also be utilized to improve the thermodynamic uncertainty relation (TUR), as recently shown in [56]. The result in Eq. (45) thus allows to inspect and understand more deeply this improved TUR.

An explicit example of the correlation result Eq. (45) for $\mathbf{C}_{\mathbf{J}\rho}^{\mathbf{xy}}(t)$ is shown in Fig. 5. In line with the previous arguing $\mathbf{C}_{\mathbf{J}\rho}^{\mathbf{xy}}(t)$ can be understood as a vector with initial- and final-point contributions, $C_{\mathbf{J}\rho}^{\mathbf{xy}}=\mathbf{C}_\mathrm{in}+\mathbf{C}_\mathrm{fi}$, where $\mathbf{C}_\mathrm{in}\equiv\hat{\mathcal{I}}_{\mathbf{xy}}^t[\hat{\mathbf{j}}_\mathbf{z}^\ddagger P_\mathbf{z}(\mathbf{z}',t')-\mathbf{j}_\mathrm{s}(\mathbf{z})p_\mathrm{s}(\mathbf{z}')]$. In the Supplemental Material of [58] we have shown that for $\mathbf{x}=\mathbf{y}$ in the limit $h\to0$ of small windows the results for the correlation simplify $\mathbf{C}_\mathrm{in}(t)\simeq[2\mathbf{j}_\mathrm{s}(\mathbf{x})/p_\mathrm{s}(\mathbf{x})-\mathbf{F}(\mathbf{x})]\mathrm{var}_\rho^\mathbf{x}(t)/4$ and $\mathbf{C}_\mathrm{fi}(t)\simeq\mathbf{F}(\mathbf{x})\mathrm{var}_\rho^\mathbf{x}(t)/4$, implying $\mathbf{C}_{\mathbf{J}\rho}^{\mathbf{xx}}(t)\simeq\mathbf{j}_\mathrm{s}(\mathbf{x})\mathrm{var}_\rho^\mathbf{x}(t)/2p_\mathrm{s}(\mathbf{x})$. Since $\mathbf{F}=\mathbf{F}^\mathrm{rev}+\mathbf{j}_\mathrm{s}/p_\mathrm{s}$ and thus $2\mathbf{j}_\mathrm{s}(\mathbf{x})/p_\mathrm{s}(\mathbf{x})-\mathbf{F}(\mathbf{x})=-\mathbf{F}^{-\mathbf{j}_\mathrm{s}}(\mathbf{x})$, the above implies that for $\mathbf{x}=\mathbf{y}$ and small windows h we have $-\mathbf{C}_\mathrm{in}=\mathbf{C}_\mathrm{fi}^{-\mathbf{j}_\mathrm{s}}$ and $\mathbf{C}_\mathrm{fi}$ points along $\mathbf{F}(\mathbf{x})$ that is tangent to the mean trajectory $[\mu]$ at $\mathbf{x}$, while $\mathbf{C}_{\mathbf{J}\rho}^{\mathbf{xx}}(t)$ points in $\mathbf{j}_\mathrm{s}(\mathbf{x})$-direction, see Fig. 5b. For longer times t and/or larger h, the direction of $\mathbf{C}_\mathrm{fi}$ changes but $-\mathbf{C}_\mathrm{in}=\mathbf{C}_\mathrm{fi}^{-\mathbf{j}_\mathrm{s}}$ still holds (see Fig. 5c) since the symmetry $\mathbf{j}_\mathrm{in}(\mathbf{y},t;\mathbf{x},0)=-\mathbf{j}_\mathrm{fi}^{-\mathbf{j}_\mathrm{s}}(\mathbf{x},t;\mathbf{y},0)$ can be applied in the integrands. Conversely, the two-point correlation $C_{\mathbf{J}\rho}^{\mathbf{xy}}$ *need not* to point along $\mathbf{j}_\mathrm{s}(\mathbf{x})$ (Fig. 5d). In fact, its direction changes over time (see inset of Fig. 5d). Notably, results for $\mathbf{x}\neq\mathbf{y}$ akin to Fig. 5d may provide deeper insight into barrier crossing problems on the level of individual trajectories in the absence of detailed balance.

F. Current (co)variance

Recall that the current (co)variance Eq. (29) involves scalar products of initial- and final-point increments $\langle\circ d\mathbf{x}_{t_1}\cdot\circ d\mathbf{x}_{t_2}\rangle_{\mathbf{x}_{t_1}=\mathbf{z}}^{\mathbf{x}_{t_2}=\mathbf{z}'}$, which *cannot* be easily interpreted as scalar products of currents. They are *not* the scalar products of initial- and final-point currents, since $\langle\circ d\mathbf{x}_{t_1}\cdot\circ d\mathbf{x}_{t_2}\rangle_{\mathbf{x}_{t_1}=\mathbf{z}}^{\mathbf{x}_{t_2}=\mathbf{z}'}\neq\langle\circ d\mathbf{x}_{t_1}\rangle_{\mathbf{x}_{t_1}=\mathbf{z}}^{\mathbf{x}_{t_2}=\mathbf{z}'}\cdot\langle\circ d\mathbf{x}_{t_2}\rangle_{\mathbf{x}_{t_1}=\mathbf{z}}^{\mathbf{x}_{t_2}=\mathbf{z}'}$. Rather they correspond to the scalar product of the initial- and final-point increment *along the same trajectory* and only then they become averaged over all trajectories from $\mathbf{z}$ to $\mathbf{z}'$ (see also Fig. 2 in [58]). For $t_1<t_2$ these are computed equivalently to Eqs. (37)-(41) based on the Lemma (36) as

$$\langle\circ d\mathbf{x}_{t_1}\cdot\circ d\mathbf{x}_{t_2}\rangle_{\mathbf{x}_{t_1}=\mathbf{z}}^{\mathbf{x}_{t_2}=\mathbf{z}'}=\hat{\mathbf{j}}_\mathbf{z}^\ddagger\cdot\hat{\mathbf{j}}_{\mathbf{z}'}P_\mathbf{z}(\mathbf{z}',t'). \quad (46)$$

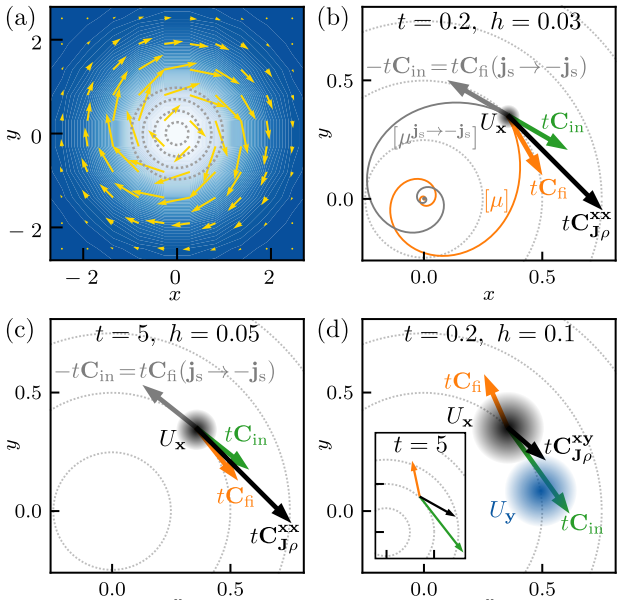

FIG. 5. (a) Illustration of the steady-state density (color gradient) and current (arrows) of the two-dimensional rotational flow Eq. (2) with $\Omega = 3$. Gray dotted lines in (a-d) are circles with radii 0.25, 0.5, 0.75, 1. (b-c) Single-point $\mathbf{x} = \mathbf{y}$ and (d) two-point time-accumulated correlation $t\mathbf{C}^{\mathbf{xy}}_{\mathbf{J}_\rho}$ at $t = 0.2$ and $t = 5$ (black arrow), with final-point $\mathbf{C}_{\rm fi} \equiv \hat{\mathcal{I}}^t_{\mathbf{xy}}[\hat{\mathbf{j}}_{\mathbf{z}} P_{\mathbf{z}'}(\mathbf{z}, t') - \mathbf{j}_{\rm s}(\mathbf{z}) p_{\rm s}(\mathbf{z}')]$ (orange) and initial-point $\mathbf{C}_{\rm in}$ (green) contribution, s. t. $\mathbf{C}^{\mathbf{xy}}_{\mathbf{J}_\rho} = \mathbf{C}_{\rm in} + \mathbf{C}_{\rm fi}$. $\mathbf{C}_{\rm fi}(\mathbf{j}_{\rm s} \to -\mathbf{j}_{\rm s})$ (gray) is the current-reversed final-point contribution which agrees with the inverted initial-point contribution $-\mathbf{C}_{\rm in}$. Full lines in (a) are the mean trajectory $[\mu] \equiv \langle \mathbf{x}_{\tau \geq 0} \rangle_{\mathbf{x}_0 = \mathbf{x}}$ (orange) and its current-reverse $[\mu^{\mathbf{j}_{\rm s} \to -\mathbf{j}_{\rm s}}]$ (gray). $U_{\mathbf{x},\mathbf{y}}$ (shaded circles) is a Gaussian at $\mathbf{x}, \mathbf{y}$ with width h, see Eq. (3).

However, according to the convention $\int_{t_1}^t dt_2 \delta(t_2 - t_1) = 1/2$ in Eq. (18), we also need to consider the case $t_1 = t_2$, i.e. $t' = 0$, which did not contribute for $C_{\rho\rho}$ and $C_{\mathbf{J}\rho}$. In the case $t_1 = t_2$ (recall the definition in Eq. (25))

$$\begin{aligned}
&\langle \circ d\mathbf{x}_{t_1} \cdot \circ d\mathbf{x}_{t_2} \rangle^{\mathbf{x}_{t_2} = \mathbf{z}'}_{\mathbf{x}_{t_1} = \mathbf{z}} \\
&\quad \equiv \langle \delta(\mathbf{x}_{t_1} - \mathbf{z}) \circ d\mathbf{x}_{t_1} \cdot \delta(\mathbf{x}_{t_2} - \mathbf{z}') \circ d\mathbf{x}_{t_2} \rangle_{\rm s} \\
&\quad \overset{t_1 = t_2}{=} \Big\langle \delta(\mathbf{x}_{t_1} - \mathbf{z}) \sqrt{2\mathbf{D}(\mathbf{x}_{t_1})} d\mathbf{W}_{t_1} \cdot \\
&\qquad \delta(\mathbf{x}_{t_2} - \mathbf{z}') \sqrt{2\mathbf{D}(\mathbf{x}_{t_2})} d\mathbf{W}_{t_2} \Big\rangle, \qquad (47)
\end{aligned}$$

where we used that for $t_1 = t_2$ the only term surviving is $d\mathbf{W}^2_{t_1}$ (and not $d\mathbf{W}_{t_1} dt_1$ and dt_1^2, which is why such terms only enter in current-current expressions but not in current-density or density-density correlations), as well as (by Itô's isometry) $\int_{t_1}^t dt_2 d\mathbf{W}^j_{t_1} \frac{d\mathbf{W}^l_{t_2}}{dt_2} = \delta_{jl} dt_1$. Using $P_{\mathbf{z}}(\mathbf{z}', t' = 0) = \delta(\mathbf{z} - \mathbf{z}') p_{\rm s}(\mathbf{z})$ we find for $t_1 = t_2$

$$\begin{aligned}
&\langle \circ d\mathbf{x}_{t_1} \cdot \circ d\mathbf{x}_{t_2} \rangle^{\mathbf{x}_{t_2} = \mathbf{z}'}_{\mathbf{x}_{t_1} = \mathbf{z}} \\
&= P_{\mathbf{z}}(\mathbf{z}', 0) \sum_{i,j,l=1}^{d} [\sqrt{2\mathbf{D}(\mathbf{z})}]_{ij} [\sqrt{2\mathbf{D}(\mathbf{z}')}]_{il} \delta(t_1 - t_2) \delta_{jl} dt_1 \\
&= p_{\rm s}(\mathbf{z}) \delta(\mathbf{z} - \mathbf{z}') \sum_{i=1}^{d} [2\mathbf{D}(\mathbf{z})]_{ii} \delta(t_1 - t_2) dt_1 \\
&= 2{\rm Tr}[\mathbf{D}(\mathbf{z})] p_{\rm s}(\mathbf{z}) \delta(\mathbf{z} - \mathbf{z}') \delta(t_1 - t_2) dt_1. \qquad (48)
\end{aligned}$$

Plugging this into Eq. (29), we obtain, using Eq. (46) and accounting for the $t' = 0$ contribution, the result for current covariances in the form of

$$\begin{aligned}
C^{\mathbf{xy}}_{\mathbf{J}\cdot\mathbf{J}}(t) &= \frac{2}{t} \int d\mathbf{z} {\rm Tr}[\mathbf{D}(\mathbf{z})] U^h_{\mathbf{x}}(\mathbf{z}) U^h_{\mathbf{y}}(\mathbf{z}) p_{\rm s}(\mathbf{z}) \qquad (49) \\
&+ \hat{\mathcal{I}}^{t,U}_{\mathbf{xy}}[\hat{\mathbf{j}}^{\ddagger}_{\mathbf{z}'} \cdot \hat{\mathbf{j}}_{\mathbf{z}} P_{\mathbf{z}'}(\mathbf{z}, t') + \hat{\mathbf{j}}^{\ddagger}_{\mathbf{z}} \cdot \hat{\mathbf{j}}_{\mathbf{z}'} P_{\mathbf{z}}(\mathbf{z}', t') - 2\mathbf{j}_{\rm s}(\mathbf{z}) \cdot \mathbf{j}_{\rm s}(\mathbf{z}')].
\end{aligned}$$

The second line is interpreted analogously to the current-density correlation in Eq. (45) with the only difference that the scalar product of current operators reflects scalar products of increments along individual trajectories. The first term, however, does not appear in $C^{\mathbf{xy}}_{\mathbf{J}\rho}$ and $C^{\mathbf{xy}}_{\rho\rho}$. As can be seen from the derivation in Eq. (48) this term originates from the purely diffusive (i.e. Brownian) term involving $d\mathbf{x}_\tau \cdot d\mathbf{x}_\tau = 2{\rm Tr}\mathbf{D}(\mathbf{z}) d\tau$ and only appears for $t_1 = t_2$, i.e. $t' = 0$. Thus, this term *cannot* be interpreted in terms of trajectories from $\mathbf{z}$ to $\mathbf{z}'$ or vice versa, but instead reflects that due to the nature of Brownian motion the square of instantaneous fluctuations $(d\mathbf{x}_\tau)^2$ does not vanish but contributes on the order $d\tau$. Note that since here $\mathbf{z} = \mathbf{z}'$ this term only contributes if $U^h_{\mathbf{x}}(\mathbf{z})$ and $U^h_{\mathbf{y}}(\mathbf{z}')$ have non-zero overlap.

For $\mathbf{x} = \mathbf{y}$ the covariance becomes the current variance ${\rm var}^{\mathbf{x}}_{\mathbf{J}}(t) \equiv C^{\mathbf{xx}}_{\mathbf{J}\cdot\mathbf{J}}(t)$ which plays a vital role in stochastic thermodynamics. As an application of the result in Eq. (49) we use the TUR-bound under concurrent variation of the coarse-graining scale h to optimize the inference of a system's dissipation via current fluctuations.

V. APPLICATION TO INFERENCE OF DISSIPATION

We now apply the results for the current variance ${\rm var}^{\mathbf{x}}_{\mathbf{J}}(t) \equiv C^{\mathbf{xx}}_{\mathbf{J}\cdot\mathbf{J}}(t)$ in Eq. (49) for $\mathbf{x} = \mathbf{y}$. For an individual component, e.g. $J_y \equiv [\overline{\mathbf{J}^U_{\mathbf{x}}}]_y$, of the vector $\overline{\mathbf{J}^U_{\mathbf{x}}}$ the equivalent result reads

$$\begin{aligned}
{\rm var}^{\mathbf{x}}_{J_y}(t) = \frac{2}{t} \int d\mathbf{z} [\mathbf{D}(\mathbf{z})]_{yy} U^h_{\mathbf{x}}(\mathbf{z}) U^h_{\mathbf{x}}(\mathbf{z}) p_{\rm s}(\mathbf{z}) + \hat{\mathcal{I}}^{t,U}_{\mathbf{xy}}[(\hat{\mathbf{j}}^{\ddagger}_{\mathbf{z}'})_y \times \\
(\hat{\mathbf{j}}_{\mathbf{z}})_y P_{\mathbf{z}'}(\mathbf{z}, t') + (\hat{\mathbf{j}}^{\ddagger}_{\mathbf{z}})_y (\hat{\mathbf{j}}_{\mathbf{z}'})_y P_{\mathbf{z}}(\mathbf{z}', t') - 2[\mathbf{j}_{\rm s}(\mathbf{z})]_y [\mathbf{j}_{\rm s}(\mathbf{z}')]_y]. \qquad (50)
\end{aligned}$$

With the dissipation rate $\dot{\Sigma}$ in Eq. (10), current observables such as $J_y \equiv [\overline{\mathbf{J}^U_{\mathbf{x}}}]_y$ satisfy the TUR [15, 34] (in the

form relevant below first proven in [15])

$$\frac{\mathrm{var}^{\mathbf{x}}_{J_y}(t)}{\langle J_y\rangle_{\mathrm{s}}^2} \geq \frac{2}{t\dot{\Sigma}}. \tag{51}$$

This bound is of particular interest since it allows to infer a lower bound on a system's dissipation from measurements of the local mean current and current fluctuations [17, 53, 73–75]. Note that Eq. (51) implicitly assumes "perfect" statistics, i.e. $\langle J_y\rangle_{\mathrm{s}}$ and $\mathrm{var}^{\mathbf{x}}_{J_y}(t)$ are the exact mean and variance for the process under consideration (not limited by sampling constraints on a finite number of realizations).

We now investigate the influence of the coarse graining on the sharpness of the bound (51). One might naively expect that coarse graining annihilates information. However, as shown in [58] the current fluctuations diverge in spatial dimensions $d \geq 2$ in the limit $h \to 0$ (of no coarse graining), whereas the mean converges to a constant (note that $\dot{\Sigma}$ does not at all depend on $U^h_{\mathbf{x}}$). The exact asymptotics for $h \to 0$ in [58] demonstrate that the bound (51) becomes entirely independent of the process (i.e. it only depends on p_{s} but contains no information about the non-equilibrium part of the dynamics). Therefore, the left hand side of the inequality (51) tends to ∞ as $h \to 0$, rendering the TUR without spatial coarse graining unable to infer dissipation beyond the statement $\dot{\Sigma} \geq 0$ for $h = 0$.

However, the naive intuition is correct in the limit of "ignorant" coarse graining $h \to \infty$, where $U^h_{\mathbf{x}}$ becomes asymptotically constant in a sufficiently large hypervolume centered at $\mathbf{x}$ (i.e. in a hypervolume A where $\int_{\mathrm{A}} p_{\mathrm{s}}(\mathbf{x})d\mathbf{x} \approx 1$). The integration over a constant $U^h_{\mathbf{x}} = c$ yields $\left\langle \overline{\mathbf{J}^U_{\mathbf{x}}}(t)\right\rangle_{\mathrm{s}} = c\int d\mathbf{z}\mathbf{j}_{\mathrm{s}}(\mathbf{z}) = \mathbf{0}$ for the mean Eq. (17). The vanishing $\left\langle \overline{\mathbf{J}^U_{\mathbf{x}}}(t)\right\rangle_{\mathrm{s}}$ may be seen in two ways. First, since $\nabla_{\mathbf{z}}\cdot\mathbf{j}_{\mathrm{s}}(\mathbf{z}) = 0$, curl $\mathbf{j}_{\mathrm{s}}(\mathbf{z}) = \nabla_{\mathbf{z}}\times\mathbf{f}(\mathbf{z})$ and by Stokes theorem $\int_{\mathrm{A}} d^2z\nabla_{\mathbf{z}}\times\mathbf{f}(\mathbf{z}) = \int_{\partial\mathrm{A}}\mathbf{f}\cdot d\mathbf{l}$ which vanishes since at the boundary ∂A at ∞ we have $p_{\mathrm{s}} \to 0$, thus $\mathbf{j}_{\mathrm{s}} \to 0$ and therefore the vector potential $\mathbf{f} \to \mathbf{0}$. Second, for $U^h_{\mathbf{x}} = c$ we have $\overline{\mathbf{J}^U_{\mathbf{x}}}(t) = \frac{c}{t}(\mathbf{x}_t - \mathbf{x}_0)$ (and we assume $\mathbf{x}_0$ to be sampled from $p_{\mathrm{s}}(\mathbf{x})$). Then $\mathbf{x}_0$ and $\mathbf{x}_t$ are both distributed according to p_{s}, thus $\langle\mathbf{x}_t\rangle_{\mathrm{s}} = \langle\mathbf{x}_0\rangle_{\mathrm{s}}$ and $t\left\langle \overline{\mathbf{J}^U_{\mathbf{x}}}(t)\right\rangle_{\mathrm{s}}/c = \langle\mathbf{x}_t\rangle_{\mathrm{s}} - \langle\mathbf{x}_0\rangle_{\mathrm{s}} = 0$. Conversely, the variance remains strictly positive. Therefore, also for $h \to \infty$ the left hand side of the inequality (51) diverges, rendering the TUR with an "ignorant" coarse graining incapable of inferring dissipation (again only gives $\dot{\Sigma} \geq 0$ as for $h = 0$).

These two arguments, i.e. the necessity of coarse graining [58] and the failure of an "ignorant" coarse graining, imply that an intermediate coarse graining exists that is optimal for inferring dissipation via the TUR (51).

We first demonstrate this finding using a two-dimensional rotational flow (2) with Gaussian coarse graining window Eq. (3). We evaluate the left hand side of Eq. (51) for varying h and $\mathbf{x}$ and compare it to the constant right hand side of Eq. (51). Particularly for $\mathbf{D}(\mathbf{z}) = D\mathbf{1}$, we have $p_{\mathrm{s}}(\mathbf{z}) = r/(2\pi D)\exp(-r\mathbf{z}^2/(2D))$ and $\mathbf{j}_{\mathrm{s}}(\mathbf{z}) = \Omega p_{\mathrm{s}}(\mathbf{z})(z_2, -z_1)^T$ and the dissipation rate Eq. (10) is given by

$$\begin{aligned}\dot{\Sigma} &= \int d\mathbf{z}\frac{\mathbf{j}_{\mathrm{s}}^T(\mathbf{z})}{p_{\mathrm{s}}(\mathbf{z})}\mathbf{D}^{-1}(\mathbf{z})\frac{\mathbf{j}_{\mathrm{s}}(\mathbf{z})}{p_{\mathrm{s}}(\mathbf{z})}p_{\mathrm{s}}(\mathbf{z}) = \frac{\Omega^2}{D}\int d\mathbf{z}\,\mathbf{z}^2 p_{\mathrm{s}}(\mathbf{z}) \\ &= \frac{\Omega^2}{D}\left\langle\mathbf{x}_0^2\right\rangle_{\mathrm{s}} = \frac{\Omega^2}{D}\left\langle x_1^2 + x_2^2\right\rangle_{\mathrm{s}} = \frac{\Omega^2}{D}2\frac{D}{r} = \frac{2\Omega^2}{r}.\end{aligned} \tag{52}$$

Thus the TUR in Eq. (51) for the rotational flow becomes

$$\frac{\mathrm{var}^{\mathbf{x}}_{J_y}(t)}{\langle J_y\rangle_{\mathrm{s}}^2} \geq \frac{r}{t\Omega^2}. \tag{53}$$

The results shown in Fig. 6a-d demonstrate, as argued above, that relative fluctuations diverge as $h \to 0, \infty$. For this example, the relative error as a function of h has a unique minimum (slightly depending on $\mathbf{x}$, and possibly on other parameters such as t). This means that (restricted to $U^h_{\mathbf{x}}$ being a Gaussian around $\mathbf{x}$) there is a coarse graining scale h that is optimal for inferring a lower bound on the dissipation, that may also provide some intuition about the formal optimization carried out in [75]. This result demonstrates that coarse graining trajectory data *a posteriori* can improve the inference of thermodynamical information, which is a strong motivation for considering coarse graining.

In particular, note that this method is readily applicable, i.e. one does not need to know the underlying process (as long as the dynamics is overdamped). As was done in Fig 6e-h one simply integrates the trajectories to obtain the coarse grained current as defined in Eq. (1). Then, the mean and variance are readily obtained from the fluctuations along an ensemble of individual trajectories, and for each value of $\mathbf{x}$ and h one determines a lower bound on the dissipation via Eq. (51). Finally, one takes the best of those bounds. We here only consider Gaussian $U^h_{\mathbf{x}}$ for the coarse graining, but due to the flexibility of the theory one could even choose window functions that do not have to relate to the notion of coarse graining. Notably, a Gaussian indicator function is in this case better than e.g. a rectangular indicator function (which one usually uses for binning data) due to an improved smoothing effect. Moreover, one further expects a reduced error due to discrete-time effects.

Note that compared to many of the similar existing methods [17, 54, 56], we *neither* advise to rasterize the continuous dynamics to parameterize (i.e. "count") currents *nor* to approximate the dynamics by a Markov-jump process, which apart from being correct (note that a Markov-jump assumption is only accurate in the presence of a time-scale separation ensuring a local equilibration, e.g. as a results of high barriers separating energy minima) has the great advantage of not having to parameterize rates at all. Instead one simply integrates trajectories according to Eq. (1).

A generalization to windows that are not centered at an individual points as well as the use of correlations in

Eq. (45) entering the recent so-called CTUR inequality [56] will be considered in forthcoming publications.

To underscore the applicability of the above inference strategy, we apply it to a more complicated system, for which a Markov jump process description would be difficult due to the presence of low and flat barriers and extended states. The results are shown Fig. 6e-h. The example is constructed by considering the two-dimensional potential

$$\begin{aligned}\phi(x,y) =&0.75(x^2-1)^2+\\ &(y^2-1.5)^2((x+0.5y-0.5)^2+0.5)+c \end{aligned} \quad (54)$$

where c is a constant such that $p_{\rm s}(\mathbf{z}) = \exp[-\phi(\mathbf{z})]$ is normalized. We consider isotropic additive noise $\mathbf{D}(\mathbf{z}) = D\mathbf{1}$ and construct the Itô/Langevin equation for the process as

$$d\mathbf{x}_\tau = -D\{\nabla\phi\}(\mathbf{x}_\tau)d\tau + \mathbf{F}^{\rm irrev}(\mathbf{x}_\tau) + \sqrt{2D}d\mathbf{W}_\tau, \quad (55)$$

where

$$\mathbf{F}^{\rm irrev}(\mathbf{z}) = \frac{\mathbf{j}_{\rm s}(\mathbf{z})}{p_{\rm s}(\mathbf{z})} \equiv -D\Omega \begin{bmatrix} 0 & -1 \\ 1 & 0 \end{bmatrix} \cdot \{\nabla\phi\}(\mathbf{z}), \quad (56)$$

is an irreversible drift that is by construction orthogonal to $\nabla\phi$ and thus does not alter the steady-state (i.e. same $p_{\rm s} = \exp[-\phi]$ for equilibrium ($\Omega = 0$) or any other Ω). With Eq. (56) the dissipation in Eq. (10) for this process reads

$$\begin{aligned}\dot\Sigma &= D\Omega^2 \int {\rm d}^2\mathbf{x} \{\nabla\phi\}(\mathbf{x})^T \begin{bmatrix} 0 & -1 \\ 1 & 0 \end{bmatrix}^T \begin{bmatrix} 0 & -1 \\ 1 & 0 \end{bmatrix} \cdot \quad (57)\\ \{\nabla\phi\}(\mathbf{x})p_s(\mathbf{x}) &= D\Omega^2 \int {\rm d}^2\mathbf{x} \{\nabla\phi\}^2(\mathbf{x}) \exp\left[-\phi(\mathbf{x})\right],\end{aligned}$$

which is solved numerically and gives $\dot\Sigma = 19.65 D\Omega^2$. We see in Fig. 6h that some intermediate coarse graining h is still optimal, but the optimal scale h now depends more intricately on $\mathbf{x}$ and the curves are not convex in h anymore.

Overall we see that the approach is robust and easily applicable, and does not require to determine and parameterize any rates. Moreover, due to the implications of the theory to the limits $h \to 0, \infty$ we can assert that some intermediate coarse graining will generally be optimal.

VI. SIMPLIFICATIONS AND SYMMETRIES

In this section we list the symmetries obeyed by the results in Eqs. (15),(17),(23),(45),(49) (with integral operator (22)). Note that the limit $h \to 0$ is carried out in [58] and the limit $h \to \infty$ gives $U^h_{\mathbf{x}} = c$ as noted before which greatly simplifies the further analysis. The limits $t \to 0$ and $t \to \infty$ will be addressed in Section VII (see also Supplemental Material in [58]).

First consider dynamics obeying detailed balance, i.e. $\mathbf{j}_{\rm s} = \mathbf{0}$. We then have $\hat{\mathbf{j}}^\dagger_{\mathbf{z}} = -\hat{\mathbf{j}}_{\mathbf{z}} = -\hat{\mathbf{j}}^g(\mathbf{z})$ and the dual-reversal symmetry in Eq. (11), simplifies to the detailed balance statement $G(\mathbf{y},t|\mathbf{x})p_{\rm s}(\mathbf{x}) = G(\mathbf{x},t|\mathbf{y})p_{\rm s}(\mathbf{y})$ or $P_{\mathbf{z}}(\mathbf{z}',t) = P_{\mathbf{z}'}(\mathbf{z},t)$. From this we obtain the following simplifications for $\mathbf{j}_{\rm s} = \mathbf{0}$:

$$\begin{aligned}&\left\langle \overline{\mathbf{J}^U_{\mathbf{x}}}(t)\right\rangle_{\rm s} = \mathbf{0}, \quad \mathbf{C}^{\mathbf{xy}}_{\mathbf{J}\rho}(t) = \mathbf{0}\\ &C^{\mathbf{xy}}_{\rho\rho}(t) = 2\hat{\mathcal{I}}^{t,U}_{\mathbf{xy}}\left[P_{\mathbf{z}}(\mathbf{z}',t') - p_{\rm s}(\mathbf{z})p_{\rm s}(\mathbf{z}')\right],\\ &C^{\mathbf{xy}}_{\mathbf{J}\cdot\mathbf{J}}(t) = \frac{2}{t}\int d\mathbf{z}{\rm Tr}[\mathbf{D}(\mathbf{z})]U^h_{\mathbf{x}}(\mathbf{z})U^h_{\mathbf{y}}(\mathbf{z})p_{\rm s}(\mathbf{z})\\ &- 2\hat{\mathcal{I}}^{t,U}_{\mathbf{xy}}[\hat{\mathbf{j}}^g(\mathbf{z})\cdot\hat{\mathbf{j}}^g(\mathbf{z}')P_{\mathbf{z}}(\mathbf{z}',t') + \mathbf{j}_{\rm s}(\mathbf{z})\cdot\mathbf{j}_{\rm s}(\mathbf{z}')]. \end{aligned} \quad (58)$$

For the remainder of this section we consider $\mathbf{j}_{\rm s} \neq \mathbf{0}$. Note that by definition the interchange $\mathbf{x} \leftrightarrow \mathbf{y}$ leaves $C^{\mathbf{xy}}_{\rho\rho}(t)$ and $C^{\mathbf{xy}}_{\mathbf{J}\cdot\mathbf{J}}(t)$ invariant, but *not* $C^{\mathbf{xy}}_{\mathbf{J}\rho}(t)$ since it considers currents at $\mathbf{x}$ and densities at $\mathbf{y}$.

For single-point correlations and variances $\mathbf{x} = \mathbf{y}$ (more precisely $U^h_{\mathbf{x}} = U^h_{\mathbf{y}}$) the integrations over $\mathbf{z}$ and $\mathbf{z}'$ are equivalent and thus the results simplify to

$$\begin{aligned}&C^{\mathbf{xx}}_{\rho\rho}(t) = 2\hat{\mathcal{I}}^{t,U}_{\mathbf{xx}}\left[P_{\mathbf{z}}(\mathbf{z}',t') - p_{\rm s}(\mathbf{z})p_{\rm s}(\mathbf{z}')\right]\\ &\mathbf{C}^{\mathbf{xx}}_{\mathbf{J}\rho}(t) = \hat{\mathcal{I}}^{t,U}_{\mathbf{xx}}[(\hat{\mathbf{j}}_{\mathbf{z}'} + \hat{\mathbf{j}}^\dagger_{\mathbf{z}})P_{\mathbf{z}}(\mathbf{z}',t') - 2\mathbf{j}_{\rm s}(\mathbf{z})p_{\rm s}(\mathbf{z}')]\\ &C^{\mathbf{xx}}_{\mathbf{J}\cdot\mathbf{J}}(t) = \frac{2}{t}\int d\mathbf{z}{\rm Tr}[\mathbf{D}(\mathbf{z})][U^h_{\mathbf{x}}]^2(\mathbf{z})p_{\rm s}(\mathbf{z})\\ &+ 2\hat{\mathcal{I}}^{t,U}_{\mathbf{xx}}[\hat{\mathbf{j}}^\dagger_{\mathbf{z}}\cdot\hat{\mathbf{j}}_{\mathbf{z}'}P_{\mathbf{z}}(\mathbf{z}',t') - \mathbf{j}_{\rm s}(\mathbf{z})\cdot\mathbf{j}_{\rm s}(\mathbf{z}')]. \end{aligned} \quad (59)$$

Now we again allow $\mathbf{x} \neq \mathbf{y}$ and consider the process and the $\mathbf{j}_{\rm s} \leftrightarrow -\mathbf{j}_{\rm s}$ inverted process. Then, from Eq. (11) and $[\hat{\mathbf{j}}^\dagger_{\mathbf{z}'}\cdot\hat{\mathbf{j}}_{\mathbf{z}}]^{-\mathbf{j}_{\rm s}} = -\hat{\mathbf{j}}_{\mathbf{z}'}\cdot[-\hat{\mathbf{j}}^\dagger_{\mathbf{z}}] = \hat{\mathbf{j}}_{\mathbf{z}'}\cdot\hat{\mathbf{j}}^\dagger_{\mathbf{z}} = \hat{\mathbf{j}}^\dagger_{\mathbf{z}}\cdot\hat{\mathbf{j}}_{\mathbf{z}'}$, we get $[\hat{\mathbf{j}}^\dagger_{\mathbf{z}'}\cdot\hat{\mathbf{j}}_{\mathbf{z}}P_{\mathbf{z}'}(\mathbf{z},t')]^{-\mathbf{j}_{\rm s}} = \hat{\mathbf{j}}^\dagger_{\mathbf{z}}\cdot\hat{\mathbf{j}}_{\mathbf{z}'}P_{\mathbf{z}}(\mathbf{z}',t')$ and thus obtain

$$\begin{aligned}\left\langle \overline{\rho^U_{\mathbf{x}}}(t)\right\rangle_{\rm s} &= \left\langle \overline{\rho^U_{\mathbf{x}}}(t)\right\rangle_{\rm s}^{-\mathbf{j}_{\rm s}}\\ \left\langle \overline{\mathbf{J}^U_{\mathbf{x}}}(t)\right\rangle_{\rm s} &= -\left\langle \overline{\mathbf{J}^U_{\mathbf{x}}}(t)\right\rangle_{\rm s}^{-\mathbf{j}_{\rm s}}\\ C^{\mathbf{xy}}_{\rho\rho}(t) &= [C^{\mathbf{xy}}_{\rho\rho}(t)]^{-\mathbf{j}_{\rm s}}\\ \mathbf{C}^{\mathbf{xy}}_{\mathbf{J}\rho}(t) &= -[\mathbf{C}^{\mathbf{xy}}_{\mathbf{J}\rho}(t)]^{-\mathbf{j}_{\rm s}}\\ C^{\mathbf{xy}}_{\mathbf{J}\cdot\mathbf{J}}(t) &= [C^{\mathbf{xy}}_{\mathbf{J}\cdot\mathbf{J}}(t)]^{-\mathbf{j}_{\rm s}}. \end{aligned} \quad (60)$$

In addition to the symmetries of the first and second cumulants, a stronger path-wise version of the dual-reversal symmetry in Eq. (11) (or time-reversal symmetry at equilibrium) dictates symmetries of the full distributions of the functionals of steady-state trajectories under the reversal $\mathbf{j}_{\rm s} \leftrightarrow -\mathbf{j}_{\rm s}$. Notably, at equilibrium ($\mathbf{j}_{\rm s} = \mathbf{0}$) these simplify to symmetries of the process (which is a much stronger result since we do not have to compare to another (artificial) process with an inverted $\mathbf{j}_{\rm s}$).

To motivate this stronger symmetry, note that for steady-state initial conditions for any finite set of times $t_1 < t_2 < \cdots < t_n$ we have that the joint density $P_n(\dots)$ for positions z_i at equally spaced times $t_i = i \times \Delta t$ for $i = 0, 1, \dots, n$ is given by (since we have a Markov process by definition, i.e. Eq. (4) has no memory)

$$\begin{aligned}&P_n(z_0,t_0;z_1,t_1;\dots;z_n,t_n)\\ &= p_{\rm s}(\mathbf{x}_0)G(\mathbf{x}_1,\Delta t|\mathbf{x}_0)\cdots G(\mathbf{x}_n,\Delta t|\mathbf{x}_{n-1}). \end{aligned} \quad (61)$$

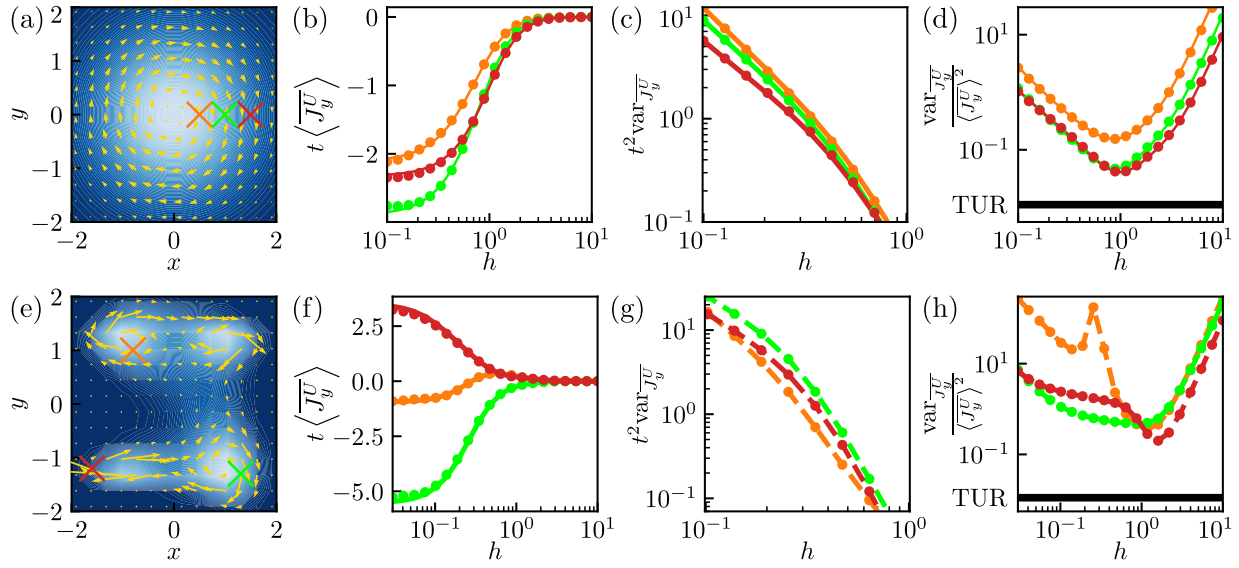

FIG. 6. (a) Steady-state density (blue color gradient) and current (yellow arrows) for the rotational flow Eq. (2) with $\Omega = 3$. Points around which the currents are evaluated in (b-d) are denoted by colored crosses. (b) Simulated values (circles) of the mean y-component of the time-integrated current from 2,000 trajectories of length $t = 10$ with time-step $dt = 0.001$ (using the stochastic Euler algorithm) starting from steady-state initial conditions using a Gaussian window function Eq. (3) with different coarse-graining scales h. Analytical results Eq. (17) are shown with lines. (c) As in (b) but for variances. Simulations (circles) are shown alongside analytical results (lines; the results are analytic up to one time-integration, see Eq. (50)) for the variance of currents. (d) The relative error (ratio of variance and mean-squared) as a function of h features a minimum at an intermediate h. At this minimum, the current fluctuations give the best lower bound on the dissipation via the TUR (51) at the value $2/(t\dot{\Sigma}) = 2/(10 \times 18) = 0.011$ (black line). (e) As in (a) but for the more complicated process in Eq. (55) with $D = 1$ and we choose $\Omega = 0.957$ to have the same dissipation as in (d); here the dissipation is obtained by means of a numerical integration. (f) As in (b) but for the process in (e) the "analytical" mean (17) had to be evaluated by means of a numerical integration. (g) As in (c) but simulated values are shown by circles and dashed line (but without a comparison to results of numerical integration since these require the knowledge of the propagator). (h) As in (d) but for the process in (e). The relative error may display several local minima. Some intermediate h still allows for an optimal inference of the dissipation via the TUR (black line). Note that the relative error diverges (orange line) where the mean crosses zero (orange line in (b)).

By applying the dual-reversal symmetry Eq. (11) $n-1$ times, we obtain

$$\begin{aligned} &P_n(z_0,t_0;z_1,t_1;\dots;z_n,t_n)\\ &= G^{-\mathbf{j}_\mathrm{s}}(\mathbf{x}_0,\Delta t|\mathbf{x}_1)\cdots G^{-\mathbf{j}_\mathrm{s}}(\mathbf{x}_{n-1},\Delta t|\mathbf{x}_n)p_\mathrm{s}(\mathbf{x}_n)\\ &= P_n^{-\mathbf{j}_\mathrm{s}}(z_n,0;z_{n-1},\Delta t;\dots;z_0,n\Delta t)\\ &= P_n^{-\mathbf{j}_\mathrm{s}}(z_n,t_0;z_{n-1},t_1;\dots;z_0,t_n). \end{aligned} \tag{62}$$

The $n+1$ points $(z_1,\dots,z_n)$ represent a discrete-time path for which Eq. (62) implies the path-wise discrete-time dual-reversal symmetry (denote $t = t_n = n\Delta t$)

$$\begin{aligned} &P_n(z_0,t_0;z_1,t_1;\dots;z_n,t_n)\\ &= P_n^{-\mathbf{j}_\mathrm{s}}(z_n,t-t_n;z_{n-1},t-t_{n-1};\dots;z_0,t-t_0), \end{aligned} \tag{63}$$

i.e. the probability of forward paths $(\mathbf{x}_{t_i})_{i=0,1,\dots,n}$ agrees with the probability of backwards paths of the process with inverted steady-state current $\mathbf{j}_\mathrm{s} \to -\mathbf{j}_\mathrm{s}$, i.e.

$$\mathbb{P}\left[(\mathbf{x}_{t_i})_{i=0,1,\dots,n}\right] = \mathbb{P}^{-\mathbf{j}_\mathrm{s}}\left[(\mathbf{x}_{t-t_i})_{i=0,1,\dots,n}\right]. \tag{64}$$

Note that at equilibrium, $\mathbf{j}_\mathrm{s} = \mathbf{0}$, this is nothing but the detailed balance for discrete-time paths.

Assuming that one can take a continuum limit $\Delta t \to 0$ (and that a resulting path measure exits) one could conclude that continuous time paths fulfill the symmetry (see also [55])

$$\mathbb{P}\left[(\mathbf{x}_\tau)_{0\le\tau\le t}\right] = \mathbb{P}^{-\mathbf{j}_\mathrm{s}}\left[(\mathbf{x}_{t-\tau})_{0\le\tau\le t}\right]. \tag{65}$$

Based on this strong symmetry, and noting that densities are symmetric while currents are antisymmetric under time reversal, i.e.

$$\begin{aligned} \overline{\rho^U_{\mathbf{x}}}\left[(x_\tau)_{0\le\tau\le t}\right] &= \overline{\rho^U_{\mathbf{x}}}\left[(x_{t-\tau})_{0\le\tau\le t}\right]\\ \overline{\mathbf{J}^U_{\mathbf{x}}}\left[(x_\tau)_{0\le\tau\le t}\right] &= -\overline{\mathbf{J}^U_{\mathbf{x}}}\left[(x_{t-\tau})_{0\le\tau\le t}\right], \end{aligned} \tag{66}$$

we obtain the following symmetries

$$\begin{aligned} \mathbb{P}\left[\overline{\rho^U_{\mathbf{x}}}(t) = u\right] &= \mathbb{P}^{-\mathbf{j}_\mathrm{s}}\left[\overline{\rho^U_{\mathbf{x}}}(t) = u\right]\\ \mathbb{P}\left[\overline{\mathbf{J}^U_{\mathbf{x}}}(t) = \mathbf{u}\right] &= \mathbb{P}^{-\mathbf{j}_\mathrm{s}}\left[\overline{\mathbf{J}^U_{\mathbf{x}}}(t) = -\mathbf{u}\right]. \end{aligned} \tag{67}$$

Eq. (67) implies symmetries for mean values and variances ($\mathbf{x} = \mathbf{y}$) listed in Eq. (60) since it implies that

all moments of $\overline{\rho^U_{\mathbf{x}}}(t)$ agree and that the n-th moment of a current component i fulfills $\left\langle [\overline{\mathbf{J}^U_{\mathbf{x}}}(t)]_i^{\,n} \right\rangle_{\mathrm{s}} = \left\langle [-\overline{\mathbf{J}^U_{\mathbf{x}}}(t)]_i^{\,n} \right\rangle_{\mathrm{s}}^{-\mathbf{j}_{\mathrm{s}}} = (-1)^n \left\langle [\overline{\mathbf{J}^U_{\mathbf{x}}}(t)]_i^{\,n} \right\rangle_{\mathrm{s}}^{-\mathbf{j}_{\mathrm{s}}}$.

Note that Eq. (67) implies that the statistics of $\rho(t)$ (incl. all moments) in general depends on $\mathbf{j}_{\mathrm{s}}$ but is invariant under the inversion $\mathbf{j}_{\mathrm{s}} \leftrightarrow -\mathbf{j}_{\mathrm{s}}$. Moreover, current fluctuations at equilibrium ($\mathbf{j}_{\mathrm{s}} = \mathbf{0}$, hence $\mathbb{P}_{\mathrm{EQ}} \equiv \mathbb{P} = \mathbb{P}^{-\mathbf{j}_{\mathrm{s}}}$) are symmetric around the mean $\left\langle \overline{\mathbf{J}^U_{\mathbf{x}}} \right\rangle_{\mathrm{s}} = \mathbf{0}$, i.e.

$$\mathbb{P}_{\mathrm{EQ}}\left[\overline{\mathbf{J}^U_{\mathbf{x}}}(t) = \mathbf{u}\right] = \mathbb{P}_{\mathrm{EQ}}\left[\overline{\mathbf{J}^U_{\mathbf{x}}}(t) = -\mathbf{u}\right]. \tag{68}$$

The symmetries for correlations in Eq. (60), possibly with $\mathbf{x} \neq \mathbf{y}$, may be seen as implications of the more general symmetries

$$\begin{aligned}
\mathbb{P}\left[\overline{\rho^U_{\mathbf{x}}}(t)\overline{\rho^U_{\mathbf{y}}}(t) = u\right] &= \mathbb{P}^{-\mathbf{j}_{\mathrm{s}}}\left[\overline{\rho^U_{\mathbf{x}}}(t)\overline{\rho^U_{\mathbf{y}}}(t) = u\right] \\
\mathbb{P}\left[\overline{\mathbf{J}^U_{\mathbf{x}}}(t)\overline{\rho^U_{\mathbf{y}}}(t) = \mathbf{u}\right] &= \mathbb{P}^{-\mathbf{j}_{\mathrm{s}}}\left[\overline{\mathbf{J}^U_{\mathbf{x}}}(t)\overline{\rho^U_{\mathbf{y}}}(t) = \mathbf{u}\right] \\
\mathbb{P}\left[\overline{\mathbf{J}^U_{\mathbf{x}}}(t)\cdot\overline{\mathbf{J}^U_{\mathbf{y}}}(t) = u\right] &= \mathbb{P}^{-\mathbf{j}_{\mathrm{s}}}\left[\overline{\mathbf{J}^U_{\mathbf{x}}}(t)\cdot\overline{\mathbf{J}^U_{\mathbf{y}}}(t) = u\right].
\end{aligned} \tag{69}$$

VII. SHORT AND LONG TRAJECTORIES AND LARGE DEVIATION THEORY

As already noted on several occasions, in the case of steady-state initial conditions the mean values of the time-averaged density and current are time-independent, see Eqs. (15),(17). The correlation and (co)variance results (Eqs. (23),(45),(49) with integral operator (22)) display a non-trivial temporal behavior dictated by the time integrals $\frac{1}{t}\int_0^t dt' \left(1 - \frac{t'}{t}\right)$ over two-point densities $P_{\mathbf{z}}(\mathbf{z}', t')$.

In Fig. 7a-c we depict this time-dependent behavior for the two-dimensional rotational flow Eq. (2) for $\mathbf{x} = \mathbf{y}$. While the short-time behavior can be obtained by analogy to the short-time expansion in the SM of [58], the long-time behavior shows that $\mathbf{C}(t), \mathrm{var}(t) \propto t^{-1}$, as expected from the central limit theorem (and large deviation theory) due to sufficiently many sufficiently uncorrelated visits of the window region. Accordingly, a serious problem is encountered in dimensions ≥ 2 in the limit $h \to 0$ because diffusive trajectories do not hit points (for a detailed discussion see [58]).

The limit of $t\mathbf{C}(t)$, $t\mathrm{var}(t)$ for large t can be obtained as follows. We have $\int_{t'}^{\infty} dt''[P_{\mathbf{y}}(\mathbf{x}, t'') - p_{\mathrm{s}}(\mathbf{x})] \to 0$ for $t' \to \infty$ since $P_{\mathbf{y}}(\mathbf{x}, t') \overset{t'\to\infty}{\longrightarrow} p_{\mathrm{s}}(\mathbf{x})$ and $\hat{\mathbf{j}}_{\mathbf{x}} P_{\mathbf{y}}(\mathbf{x}, t') \overset{t'\to\infty}{\longrightarrow} \mathbf{j}_{\mathrm{s}}(\mathbf{x})$ with exponentially decaying deviations. This implies that for large t, we can replace $\frac{1}{t}\int_0^t dt' \left(1 - \frac{t'}{t}\right)$ by $\frac{1}{t}\int_0^{\infty} dt'$ in the integral operator (22). This replacement of integrals and the scaling are also confirmed by a spectral expansion (see e.g. [51] for spectral-theoretic results for the empirical density).

We now enter the realms of large deviation theory. According to the central limit theorem (for strictly positive h, see [58]), the probability distributions $p(A_t = a)$ for $A_t = \overline{\rho^U_{\mathbf{x}}}(t)$ and $A_t = \overline{\mathbf{J}^U_{\mathbf{x}}}(t)$ become Gaussian for large t, such that we obtain the large deviation rate function

$$I(a) = -\lim_{t\to\infty} \frac{1}{t} \ln p(A_t = a) = \frac{(a-\mu)^2}{2\sigma_A^2}, \tag{70}$$

where the mean μ is given by $\left\langle \rho^U_{\mathbf{x}}(t) \right\rangle_{\mathrm{s}} = \int d^d z U^h_{\mathbf{x}}(\mathbf{z}) p_{\mathrm{s}}(\mathbf{z})$ and $\left\langle \mathbf{J}^U_{\mathbf{x}}(t) \right\rangle_{\mathrm{s}} = \int d^d z U^h_{\mathbf{x}}(\mathbf{z}) \mathbf{j}_{\mathrm{s}}(\mathbf{z})$ (see Eqs. (15),(17)) and the large deviation variance σ_A^2 follows by the above arguments from Eqs. (23) and (49) for $\mathbf{x} = \mathbf{y}$ as in Eq. (59) as

$$\begin{aligned}
\sigma^2_{\overline{\rho^U_{\mathbf{x}}}} &\equiv \lim_{t\to\infty} t\,\mathrm{var}^{\mathbf{x}}_{\rho}(t) \\
&= 2\int_0^{\infty} dt' \int d^d z \int d^d z' U^h_{\mathbf{x}}(\mathbf{z}) U^h_{\mathbf{x}}(\mathbf{z}') \\
&\quad \times \left[P_{\mathbf{z}'}(\mathbf{z}, t) - p_{\mathrm{s}}(\mathbf{z}) p_{\mathrm{s}}(\mathbf{z}')\right],
\end{aligned} \tag{71}$$

as well as

$$\begin{aligned}
\sigma^2_{\overline{\mathbf{J}^U_{\mathbf{x}}}} &\equiv \lim_{t\to\infty} t\,\mathrm{var}^{\mathbf{x}}_{\mathbf{J}}(t) = 2\mathrm{Tr}\mathbf{D} \int d^d z\, [U^h_{\mathbf{x}}]^2(\mathbf{z}) p_{\mathrm{s}}(\mathbf{z}) \\
&+ 2\int_0^{\infty} dt' \int d^d z \int d^d z' U^h_{\mathbf{x}}(\mathbf{z}) U^h_{\mathbf{x}}(\mathbf{z}') \\
&\quad \times \left[\hat{\mathbf{j}}_{\mathbf{z}} \cdot \hat{\mathbf{j}}^{\ddagger}_{\mathbf{z}'} P_{\mathbf{z}'}(\mathbf{z}, t) - \mathbf{j}_{\mathrm{s}}(\mathbf{z}) \mathbf{j}_{\mathrm{s}}(\mathbf{z}')\right].
\end{aligned} \tag{72}$$

For any Lebesgue integrable window function $U^h_{\mathbf{x}}$ (i.e. if the window size h fulfills $h > 0$), and in $d = 1$ even for the delta-function (see SM of [58]), this variance is finite, and the central limit theorem applies as described above. The parabolic rate function for a two dimensional system with finite window size $h > 0$ is shown for the density $\overline{\rho^U_{\mathbf{x}}}(t)$ and current $\overline{\mathbf{J}^U_{\mathbf{x}}}(t)$ in Fig. 7e and g. The agreement of the simulation and the variance given by Eqs. (71)-(72) is readily confirmed.

VIII. CONCLUSION

In this extended exposé accompanying the Letter [58] we presented the conceptual and technical background that is required to describe and understand the statistics of the empirical density and current of steady-state diffusions, which are central to statistical mechanics and thermodynamics on the level of individual trajectories. In order to gain deeper insight into the meaning of fluctuations of the empirical density and current we made use of a generalized time-reversal symmetry. We carried out a systematic analysis of the effect of a spatial coarse graining. A systematic variation of the coarse-graining scale in an *a posteriori* smoothing of trajectory data was proposed as an efficient method to infer bounds on a system's dissipation. Moreover, we discussed symmetries in the statistics of the empirical current and density that

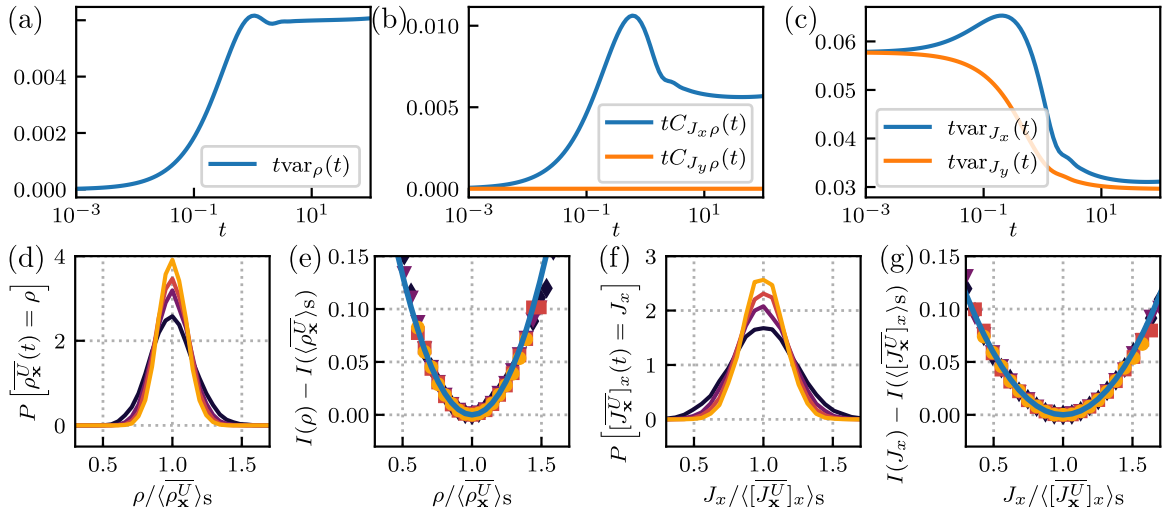

FIG. 7. We consider the rotational flow Eq. (2) with $\Omega = 3$ starting from steady-state initial conditions and use a Gaussian coarse-graining window Eq. (3) around $\mathbf{x} = (0,1)^T$ with width $h = 0.5$. (a) Analytical result for the variance of the time-averaged density $\overline{\rho^U_{\mathbf{x}}(t)}$ multiplied by time t as a function of t. At long times the variance approaches the large deviation variance in Eq. (72). (b) As in (a) but for the components of the correlation vector $\mathbf{C}^{\mathbf{xx}}_{\mathbf{J}\rho}(t)$ as in Eqs. (45) and (59). (c) As in (a) but for the variances of the current components Eq. (50). (d) Simulation of the probability density function of the empirical density $\overline{\rho^U_{\mathbf{x}}}(t)$ assuming the parameters listed above. Colors of lines and symbols throughout denote $t = 40, 60, 80, 100$ from dark to bright. The simulated probability densities were obtained from histograms of 2×10^4 trajectories for each set of parameters. (e) Parabolic rate function with variance from Eq. (72) (line) and simulated rate function $I(\rho) = -\frac{1}{t}\ln P[\overline{\rho^U_{\mathbf{x}}}(t) = \rho]$ (symbols). The numerical value of the rate function at the mean $\rho = \langle\overline{\rho^U_{\mathbf{x}}}(t)\rangle_s$ was subtracted. (f-g) As in (d-e) but for the x-component of the current $[\overline{\mathbf{J}^U_{\mathbf{x}}}]_x$ instead of the density $\overline{\rho^U_{\mathbf{x}}}$.

arise as a result of the (generalized) time-reversal symmetry. Throughout the work we advocated the application of stochastic calculus, which is very powerful in the analysis of related problems and represents a more direct alternative to Feynman-Kac theory and path-integral methods. The technical background and concepts presented here may serve as a basis for forthcoming publications, including the generalization of the presented inference strategy to windows that are not centered at an individual point, as well as the use of the correlations result entering the CTUR inequality [56].

Acknowledgments—Financial support from Studienstiftung des Deutschen Volkes (to C. D.) and the German Research Foundation (DFG) through the Emmy Noether Program GO 2762/1-2 (to A. G.) is gratefully acknowledged.

[1] T. Bodineau and B. Derrida, Current fluctuations in nonequilibrium diffusive systems: An additivity principle, Phys. Rev. Lett. **92**, 180601 (2004).
[2] L. Bertini, A. D. Sole, D. Gabrielli, G. Jona-Lasinio, and C. Landim, Current fluctuations in stochastic lattice gases, Phys. Rev. Lett. **94**, 030601 (2005).
[3] R. K. P. Zia and B. Schmittmann, Probability currents as principal characteristics in the statistical mechanics of non-equilibrium steady states, J. Stat. Mech: Theory Exp. , 07012 (2007).
[4] C. Maes, K. Netočný, and B. Wynants, Steady state statistics of driven diffusions, Physica A **387**, 2675 (2008).
[5] T. R. Gingrich, J. M. Horowitz, N. Perunov, and J. L. England, Dissipation bounds all steady-state current fluctuations, Phys. Rev. Lett. **116**, 120601 (2016).
[6] C. Maes and K. Netočný, Canonical structure of dynamical fluctuations in mesoscopic nonequilibrium steady states, EPL (Europhys. Lett.) **82**, 30003 (2008).
[7] A. C. Barato and R. Chetrite, A formal view on level 2.5 large deviations and fluctuation relations, J. Stat. Phys. **160**, 1154 (2015).
[8] M. Baiesi, C. Maes, and K. Netočný, Computation of current cumulants for small nonequilibrium systems, J. Stat. Phys. **135**, 57 (2009).
[9] V. Y. Chernyak, M. Chertkov, S. V. Malinin, and R. Teodorescu, Non-equilibrium thermodynamics and topology of currents, J. Stat. Phys. **137**, 109 (2009).
[10] L. Bertini, A. D. Sole, D. Gabrielli, G. Jona-Lasinio, and C. Landim, Macroscopic fluctuation theory, Rev. Mod. Phys. **87**, 593 (2015).
[11] P. Pietzonka, A. C. Barato, and U. Seifert, Universal bounds on current fluctuations, Phys. Rev. E **93**, 052145 (2016).
[12] T. R. Gingrich and J. M. Horowitz, Fundamental bounds on first passage time fluctuations for currents, Phys. Rev. Lett. **119**, 170601 (2017).
[13] A. C. Barato, R. Chetrite, A. Faggionato, and

D. Gabrielli, Bounds on current fluctuations in periodically driven systems, New J. Phys. **20**, 103023 (2018).
[14] M. Kaiser, R. L. Jack, and J. Zimmer, Canonical structure and orthogonality of forces and currents in irreversible Markov chains, J. Stat. Phys. **170**, 1019 (2018).
[15] A. Dechant and S.-i. Sasa, Current fluctuations and transport efficiency for general Langevin systems, J. Stat. Mech. , 063209 (2018).
[16] C. Battle, C. P. Broedersz, N. Fakhri, V. F. Geyer, J. Howard, C. F. Schmidt, and F. C. MacKintosh, Broken detailed balance at mesoscopic scales in active biological systems, Science **352**, 604 (2016).
[17] J. Li, J. M. Horowitz, T. R. Gingrich, and N. Fakhri, Quantifying dissipation using fluctuating currents, Nat. Commun. **10**, 1666 (2019).
[18] É. Roldán and J. M. R. Parrondo, Estimating dissipation from single stationary trajectories, Phys. Rev. Lett. **105**, 150607 (2010).
[19] L. Dabelow, S. Bo, and R. Eichhorn, Irreversibility in active matter systems: Fluctuation theorem and mutual information, Phys. Rev. X **9**, 021009 (2019).
[20] S. Pigolotti, I. Neri, É. Roldán, and F. Jülicher, Generic properties of stochastic entropy production, Phys. Rev. Lett. **119**, 140604 (2017).
[21] U. Seifert, Stochastic thermodynamics, fluctuation theorems and molecular machines, Rep. Prog. Phys. **75**, 126001 (2012).
[22] U. Seifert, Entropy production along a stochastic trajectory and an integral fluctuation theorem, Phys. Rev. Lett. **95**, 040602 (2005).
[23] M. Esposito and C. Van den Broeck, Three faces of the second law. I. Master equation formulation, Phys. Rev. E **82**, 011143 (2010).
[24] C. Van den Broeck and M. Esposito, Three faces of the second law. II. Fokker-Planck formulation, Phys. Rev. E **82**, 011144 (2010).
[25] S. Vaikuntanathan and C. Jarzynski, Dissipation and lag in irreversible processes, EPL (Europhys. Lett.) **87**, 60005 (2009).
[26] H. Qian, A decomposition of irreversible diffusion processes without detailed balance, J. Math. Phys. **54**, 053302 (2013).
[27] A. Lapolla and A. Godec, Faster uphill relaxation in thermodynamically equidistant temperature quenches, Phys. Rev. Lett. **125**, 110602 (2020).
[28] C. Maes, K. Netočný, and B. Wynants, Monotonic return to steady nonequilibrium, Phys. Rev. Lett. **107**, 010601 (2011).
[29] C. Maes, Frenetic bounds on the entropy production, Phys. Rev. Lett. **119**, 160601 (2017).
[30] N. Shiraishi and K. Saito, Information-theoretical bound of the irreversibility in thermal relaxation processes, Phys. Rev. Lett. **123**, 110603 (2019).
[31] T. Koyuk and U. Seifert, Thermodynamic uncertainty relation for time-dependent driving, Phys. Rev. Lett. **125**, 260604 (2020).
[32] D.-Q. Jiang, M. Qian, and M.-P. Qian, *Mathematical Theory of Nonequilibrium Steady States* (Springer Berlin Heidelberg, 2004).
[33] U. Seifert and T. Speck, Fluctuation-dissipation theorem in nonequilibrium steady states, EPL (Europhys. Lett.) **89**, 10007 (2010).
[34] A. C. Barato and U. Seifert, Thermodynamic uncertainty relation for biomolecular processes, Phys. Rev. Lett. **114**, 158101 (2015).
[35] C. Schroeder, R. Teixeira, E. Shaqfeh, and S. Chu, Characteristic periodic motion of polymers in shear flow, Phys. Rev. Lett. **95**, 018301 (2005).
[36] M. Harasim, B. Wunderlich, O. Peleg, M. Kröger, and A. R. Bausch, Direct observation of the dynamics of semiflexible polymers in shear flow, Phys. Rev. Lett. **110**, 108302 (2013).
[37] S. Gerashchenko and V. Steinberg, Statistics of tumbling of a single polymer molecule in shear flow, Phys. Rev. Lett. **96**, 038304 (2006).
[38] A. Alexander-Katz, M. F. Schneider, S. W. Schneider, A. Wixforth, and R. R. Netz, Shear-flow-induced unfolding of polymeric globules, Phys. Rev. Lett. **97**, 138101 (2006).
[39] H. Qian and M. Qian, Pumped biochemical reactions, nonequilibrium circulation, and stochastic resonance, Phys. Rev. Lett. **84**, 2271 (2000).
[40] H. Qian, Phosphorylation energy hypothesis: Open chemical systems and their biological functions, Annu. Rev. Phys. Chem. **58**, 113 (2007).
[41] S. Toyabe, T. Okamoto, T. Watanabe-Nakayama, H. Taketani, S. Kudo, and E. Muneyuki, Nonequilibrium energetics of a single $\mathbf{f}_1$-ATPase molecule, Phys. Rev. Lett. **104**, 198103 (2010).
[42] M. C. Marchetti, J. F. Joanny, S. Ramaswamy, T. B. Liverpool, J. Prost, M. Rao, and R. A. Simha, Hydrodynamics of soft active matter, Rev. Mod. Phys. **85**, 1143 (2013).
[43] N. Fakhri, A. D. Wessel, C. Willms, M. Pasquali, D. R. Klopfenstein, F. C. MacKintosh, and C. F. Schmidt, High-resolution mapping of intracellular fluctuations using carbon nanotubes, Science **344**, 1031 (2014).
[44] É. Fodor, C. Nardini, M. E. Cates, J. Tailleur, P. Visco, and F. van Wijland, How far from equilibrium is active matter?, Phys. Rev. Lett. **117**, 038103 (2016).
[45] J. Gladrow, N. Fakhri, F. C. MacKintosh, C. F. Schmidt, and C. P. Broedersz, Broken detailed balance of filament dynamics in active networks, Phys. Rev. Lett. **116**, 248301 (2016).
[46] F. S. Gnesotto, F. Mura, J. Gladrow, and C. P. Broedersz, Broken detailed balance and non-equilibrium dynamics in living systems: a review, Rep. Prog. Phys. **81**, 066601 (2018).
[47] F. Ritort, Single-molecule experiments in biological physics: methods and applications, J. Phys.: Cond. Matt. **18**, R531 (2006).
[48] W. J. Greenleaf, M. T. Woodside, and S. M. Block, High-resolution, single-molecule measurements of biomolecular motion, Annu. Rev. Biophys. Biomol. Struct. **36**, 171 (2007).
[49] J. R. Moffitt, Y. R. Chemla, S. B. Smith, and C. Bustamante, Recent advances in optical tweezers, Annu. Rev. Biochem. **77**, 205 (2008).
[50] S. Burov, J.-H. Jeon, R. Metzler, and E. Barkai, Single particle tracking in systems showing anomalous diffusion: the role of weak ergodicity breaking, Phys. Chem. Chem. Phys. **13**, 1800 (2011).
[51] A. Lapolla, D. Hartich, and A. Godec, Spectral theory of fluctuations in time-average statistical mechanics of reversible and driven systems, Phys. Rev. Research **2**, 043084 (2020).

[52] H. Qian, Nonequilibrium steady-state circulation and heat dissipation functional, Phys. Rev. E **64**, 022101 (2001).

[53] J. M. Horowitz and T. R. Gingrich, Thermodynamic uncertainty relations constrain non-equilibrium fluctuations, Nat. Phys. **16**, 15 (2019).

[54] T. R. Gingrich, G. M. Rotskoff, and J. M. Horowitz, Inferring dissipation from current fluctuations, J. Phys. A: Math. Theor. **50**, 184004 (2017).

[55] A. Dechant and S.-i. Sasa, Continuous time reversal and equality in the thermodynamic uncertainty relation, Phys. Rev. Research **3**, 042012 (2021).

[56] A. Dechant and S.-i. Sasa, Improving thermodynamic bounds using correlations, Phys. Rev. X **11**, 041061 (2021).

[57] An ergodic time scale is longer than any correlation time in the system.

[58] C. Dieball and A. Godec, Mathematical, thermodynamical, and experimental necessity for coarse graining empirical densities and currents in continuous space (2022), arXiv:2105.10483 [cond-mat.stat-mech].

[59] R. Durrett, *Stochastic calculus: A practical introduction*, 1st ed. (CRC Press, Boca Raton, 1996).

[60] A. Dechant, Multidimensional thermodynamic uncertainty relations, J. Phys. A: Math. Theor. **52**, 035001 (2018).

[61] A. Dechant and S.-i. Sasa, Fluctuation–response inequality out of equilibrium, Proc. Natl. Acad. Sci. U.S.A. **117**, 6430 (2020).

[62] C. W. Gardiner, *Handbook of stochastic methods for physics, chemistry, and the natural sciences* (Springer-Verlag, Berlin New York, 1985).

[63] G. A. Pavliotis, *Stochastic Processes and Applications* (Springer New York, 2014).

[64] D. Hartich and A. Godec, Emergent memory and kinetic hysteresis in strongly driven networks, Phys. Rev. X **11**, 041047 (2021).

[65] P. Hänggi and H. Thomas, Stochastic processes: Time evolution, symmetries and linear response, Phys. Rep. **88**, 207 (1982).

[66] Y. Klimontovich, Ito, stratonovich and kinetic forms of stochastic equations, Physica A **163**, 515 (1990).

[67] A. Lapolla and A. Godec, Manifestations of projection-induced memory: General theory and the tilted single file, Front. Phys. **7**, 182 (2019).

[68] R. E. Spinney and I. J. Ford, Entropy production in full phase space for continuous stochastic dynamics, Phys. Rev. E **85**, 051113 (2012).

[69] T. Hatano and S.-i. Sasa, Steady-state thermodynamics of Langevin systems, Phys. Rev. Lett. **86**, 3463 (2001).

[70] D. Carbone and L. Rondoni, Necessary and sufficient conditions for time reversal symmetry in presence of magnetic fields, Symmetry **12**, 1336 (2020).

[71] H. Risken, *The Fokker-Planck Equation* (Springer Berlin Heidelberg, 1996).

[72] D. A. Darling and M. Kac, On occupation times for Markoff processes, Trans. Am. Math. Soc. **84**, 444 (1957).

[73] S. K. Manikandan, D. Gupta, and S. Krishnamurthy, Inferring entropy production from short experiments, Phys. Rev. Lett. **124**, 120603 (2020).

[74] S. Otsubo, S. Ito, A. Dechant, and T. Sagawa, Estimating entropy production by machine learning of short-time fluctuating currents, Phys. Rev. E **101**, 062106 (2020).

[75] T. V. Vu, V. T. Vo, and Y. Hasegawa, Entropy production estimation with optimal current, Physical Review E **101**, 042138 (2020).